

1 **Evaporation and water sourcing dominate lake and stream isotopic variability**
2 **across time and space in a High Arctic periglacial landscape**

3 **Pete D. Akers¹, Ben G. Kopec², Eric S. Klein³, Jeffrey M. Welker^{2,4,5}**

4 ¹Discipline of Geography, School of Natural Sciences, Trinity College Dublin, Dublin,
5 Ireland.

6 ²Ecology and Genetics Research Unit, University of Oulu, 90014 Oulu, Finland.

7 ³Department of Geological Sciences, University of Alaska Anchorage, Anchorage, AK, USA.

8 ⁴Department of Biological Sciences, University of Alaska Anchorage, Anchorage, AK, USA.

9 ⁵University of the Arctic (UArctic), c/o University of Lapland, 96101 Rovaniemi, Finland.

10

11 Corresponding author: Pete D. Akers (pete.akers@tcd.ie)

12

13 **Key Points:**

- 14 • 535 water isotope samples taken over two years in Pituffik, Greenland, provide
15 exceptional insight into High Arctic isotope hydrology.
- 16 • Lake isotopes vary with evaporation and snowpack melt while stream isotopes reflect
17 relative sourcing of snowpack vs. ice sheet meltwater.
- 18 • For paleoclimate applications, lakes should be monitored frequently for isotopes for
19 as long as possible as part of a regional lake suite.
- 20

21 **Abstract**

22 Rapidly changing climate is disrupting the High Arctic's natural water systems. This
23 disruption demands high quality monitoring of Arctic hydrology to better reconstruct past
24 changes, track ongoing transformations, and assess future environmental threats. Water
25 isotopes are valuable tracers of hydrological processes, but logistical challenges limit the
26 length and scope of isotopic monitoring in High Arctic landscapes. Here, we present a
27 comprehensive isotopic survey of 535 water samples taken in 2018–2019 of the lakes,
28 streams, and other surface waters of the periglacial Pituffik Peninsula in far northwest
29 Greenland. The $\delta^{18}\text{O}$, $\delta^2\text{H}$, and deuterium-excess values of these samples, representing 196
30 unique sites, grant us unprecedented insight into the environmental drivers of the region's
31 hydrology and water isotopic variability. We find that the spatial and temporal variability of
32 lake isotopes is dominated by evaporation and connectivity to summer meltwater sources,
33 while evaporation determines interannual isotopic changes. Stream isotopic compositions
34 vary in both space and time based on the relative source balance of tundra snowpack
35 meltwater versus surface melt from the nearby Greenland Ice Sheet. Overall, our survey
36 highlights the diversity of isotopic composition and evolution in Pituffik surface waters, and
37 our complete isotopic and geospatial database provides a strong foundation for future
38 researchers to study hydrological changes at Pituffik and across the Arctic. Water isotope
39 samples taken at individual times or sites in similar periglacial landscapes likely have limited
40 regional representativeness, and increasing the spatiotemporal extent of isotopic sampling is
41 critical to producing accurate and informative High Arctic paleoclimate reconstructions.

42 **Plain language summary**

43 The isotopes of water can help us track how rapidly changing climate is disrupting High
44 Arctic water systems, but the challenging Arctic environment has limited the monitoring
45 required to understand its water isotopes. To address this, we collected 535 water isotope
46 samples from lakes, streams, and other waters on the Pituffik Peninsula in northwest
47 Greenland in 2018 and 2019. We found that differences in lake isotopes are mainly due to
48 water evaporation and how connected a lake is to sources of meltwater in the summer. These
49 two factors produce clear patterns in isotopes that we observe over both time and space. The
50 isotopic composition of streams, on the other hand, varies based on the balance of their water
51 that is coming from either melting tundra snow or from melt of the nearby Greenland Ice

52 Sheet. Our study highlights the varied isotopic makeup of water in the Pituffik area. The
 53 information we collected about isotopes is a good starting point for other scientists who want
 54 to study how water is changing, not just in Pituffik, but also in the whole Arctic. Our findings
 55 tell us that if we only collect water samples once or twice, or only in one place, we might not
 56 get the full picture of what is happening with the isotopes across the whole region. To get a
 57 better understanding of how the climate is changing in the High Arctic, it's crucial to collect
 58 isotopic samples from a wider range of locations and over longer periods of time.

59 **1 Introduction**

60 Anthropogenic climate change is transforming periglacial water systems in the Arctic by
 61 shifting the seasonality, intensity, and sources of precipitation, thawing permafrost,
 62 increasing surface evaporation, and lengthening snow- and ice-free summers (Bailey et al.,
 63 2021; Bintanja & Selten, 2014; Box et al., 2019; Farquharson et al., 2019; Lupascu et al.,
 64 2014; Mellat et al., 2021; Vonk et al., 2015). These transformations are greatly disrupting
 65 existing ecosystems and biogeochemical cycles (e.g., N. J. Anderson et al., 2017; Bhatt et al.,
 66 2017; Buchwal et al., 2020; Gimeno et al., 2019; Hiltunen et al., 2022), as well as threatening
 67 long-established livelihoods of indigenous Arctic communities (Hauser et al., 2021; Wesche
 68 & Chan, 2010). Despite the Arctic experiencing some of the most rapid climate change on
 69 Earth (Serreze & Barry, 2011), Arctic freshwater systems (e.g., lakes, streams, supra-
 70 permafrost flow) are lesser studied and monitored than systems in other regions of the world
 71 due to their remoteness, harsh environments, and relatively lower magnitude of use by human
 72 populations (Linderholm et al., 2018). As a result, this lack of baseline studies and data can
 73 make it difficult to quantify how the hydrology of an Arctic region has changed or is
 74 currently changing.

75 Here, we provide one such baseline study through a foundational overview of the
 76 hydrological structure and stable isotopic variability of the surface freshwater system across
 77 the periglacial Pituffik Peninsula in northwest Greenland. The stable isotopic composition of
 78 water (discussed here through $\delta^{18}\text{O}$ and $\delta^2\text{H}$, where $\delta = \frac{R_{\text{sample}}}{R_{\text{standard}}} - 1$ and R is the measured
 79 ratio of rare to abundant isotopologue, and through deuterium-excess (dxs), where $dxs = \delta^2\text{H}$
 80 $- 8 * \delta^{18}\text{O}$) can assist in quantifying the fundamental properties and processes of the Arctic
 81 environment by serving as key environmental tracers for water throughout its hydrological
 82 cycle history (Craig, 1961; Dansgaard, 1964; Gat, 1996; Gonfiantini, 1986; Rozanski et al.,

83 1993). This tracing is possible because water molecules containing heavier isotopes of
84 oxygen and/or hydrogen are discriminated against through kinetic fractionation during phase
85 transitions from solid to liquid to vapor and favored during the reverse of these transitions.
86 This fractionation leads to a strong linear relationship in oxygen and hydrogen isotopic ratios
87 in precipitation that is described globally with the global meteoric water line (GMWL) where
88 $\delta^2\text{H} = 8 * \delta^{18}\text{O} + 10 \text{‰}$ (Craig, 1961) and locally with local meteoric water lines (LMWL)
89 (Putman et al., 2019; Rozanski et al., 1993). Additionally, diffusion across a humidity
90 gradient during evaporation can slightly favor the vapor phase enrichment of H^2HO relative
91 to the more slowly diffusing H_2^{18}O molecule, and the impact of this nonequilibrium process
92 can be quantified through the second-order isotopic parameter of dxs (Craig & Gordon, 1965;
93 Merlivat & Jouzel, 1979). For open bodies of water that experience sustained evaporative
94 losses, this nonequilibrium process means that their $\delta^2\text{H}$ vs. $\delta^{18}\text{O}$ values will plot along a
95 local evaporation line (LEL) that falls below the GMWL and LMWL in $\delta^2\text{H}$ – $\delta^{18}\text{O}$ space (i.e.,
96 the slope of the $\delta^2\text{H}$ vs. $\delta^{18}\text{O}$ relationship will be lower than the slopes of the GMWL and
97 LMWL).

98 Due to these isotopic processes, the stable isotopic ratios and dxs values of two identical
99 source waters will diverge from each other as they experience different histories of
100 evaporation, condensation, and transportation. As a result, water isotopic compositions have
101 been harnessed with great success in the Arctic to identify moisture sources of precipitation
102 and water vapor (e.g., Akers et al., 2020; Bailey et al., 2021; Bonne et al., 2014; Kopec et al.,
103 2019; Mellat et al., 2021), estimate lake water balances (e.g., L. Anderson et al., 2013; Arp et
104 al., 2015; Cluett & Thomas, 2020; Gibson & Reid, 2014), examine plant ecophysiology (e.g.,
105 Jespersen et al., 2018; Muhic et al., 2023), and reconstruct past climate (e.g., Daniels et al.,
106 2021; Lasher et al., 2017; MacGregor et al., 2020; McFarlin et al., 2019). Provided that the
107 isotopic ratios of an initial water source supply are known or can be estimated, the isotopic
108 ratios of environmental waters in lakes, streams, and the subsurface can also be used to track
109 water movement and calculate hydrological budgets across the landscape (e.g., Bowen et al.,
110 2018; I. D. Clark & Fritz, 1997; Gibson et al., 2016; Kendall & McDonnell, 1998; Noor et
111 al., 2023; Wilcox et al., 2022).

112 This study presents isotopic data for over 500 individual water samples from 200 unique sites
113 across the Pituffik Peninsula along with an associated hydrological geospatial database.
114 Together, our data offer a spatially and temporally detailed snapshot of a largely intact High

115 Arctic hydrological landscape in the early 21st century. Through this nearly complete
116 systematic sampling of Pituffik water bodies over two consecutive summers, we provide a
117 comprehensive baseline dataset of the lakes, streams, and other surface waters in our large
118 study region (>800 km²) that can serve as a high-quality reference for contemporary and
119 future circumpolar studies. We use these survey data to determine the environmental drivers
120 of lake and stream isotopes in the Pituffik freshwater system for broader application to
121 analogous water systems across the Arctic.

122 Many paleoenvironmental studies using natural archives of oxygen and hydrogen isotopes in
123 sediments must assume typical water isotopic values from local water isotopic monitoring to
124 reconstruct past environmental changes (e.g., McFarlin et al., 2019; Sauer et al., 2001;
125 Verbruggen et al., 2011). However, the logistical challenges of Arctic field work often force
126 these assumptions to be based on limited monitoring data, and inferences and conclusions
127 made in light of such data risk inaccuracy and misinterpretation if the monitoring data were
128 not truly representative of local and/or regional isotopic norms. Therefore, the comprehensive
129 nature of our Pituffik isotopic survey gives light to the general natural variability that exists
130 in Arctic surface water isotopic systems across both time and space, and we use this
131 knowledge to advise best practices for paleoenvironmental researchers working in similar
132 environments. Overall, our insight into the isotopic variability of this High Arctic periglacial
133 water system offers great potential for researchers using isotopic proxies for reconstructing
134 both past and current environmental change as well as providing future researchers a
135 reference point to examine how much the environment will have changed since the early 21st
136 century.

137

138 **2 Geographic overview of the Pituffik region**

139 Our study focuses on the “Pituffik region” of northwest Greenland which we define here as
140 synonymous with the Pituffik Peninsula and its nearby offshore waters (Figure 1). A full
141 understanding of the modern hydrology of the region must be grounded in the context of its
142 environmental and human history. The region covers roughly 880 km² of ice-free land
143 bounded by the Greenland Ice Sheet (GrIS) to the east, Baffin Bay and Bylot Sound to the
144 west, and Uummannaq Kangerlua (Wolstenholme Fjord) to the north (76.25–76.60 °N,
145 67.60–69.70 °W). This region is also commonly referred to as the “Thule area” in reference

146 to the original Danish placename and a subsequent local United States military base. Place
147 names throughout this text will be given in the following priority as known: indigenous
148 Greenlandic names first (Oqaasileriffik, 2022), followed by common English and Danish
149 names, and finally informal names assigned by the authors to features with no known existing
150 names.

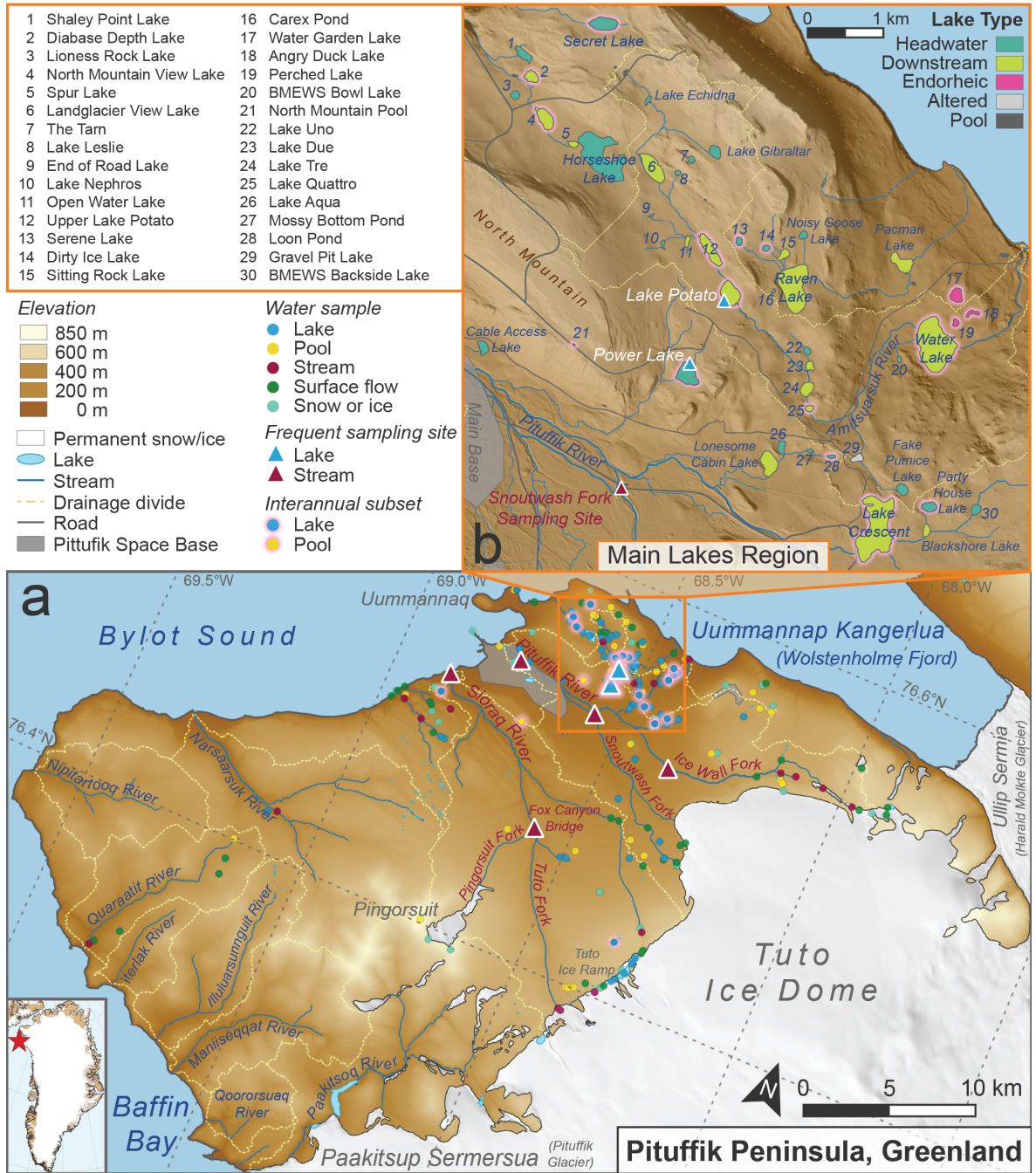
151 The landscape of the Pituffik Peninsula has long been noted for its numerous distinctive
152 landmarks, including the flat-topped Uummanaq (Mount Dundas), the easily accessed
153 “Tuto” margin of the GrIS, and the broad, formerly ecologically productive valley now filled
154 by Pituffik Space Base (Figure 1a). The southern and western parts of the peninsula consist of
155 relatively gently sloped uplands culminating in the 815 m Pingorsuit massif, while the
156 northern part of the peninsula near the military base has many broad ridges, steep-faced
157 outcrops, and lakes interspersed on a wide plain that steadily rises eastward toward the local
158 Tuto ice dome of the GrIS (Davies & Reitzel, 1963). The Tuto dome itself covers $\approx 1000 \text{ km}^2$
159 with maximum elevations over 1000 m. Although connected to the main GrIS, the Tuto dome
160 has a largely independent mass balance regulated by local precipitation, extensive summer
161 surface melt, and discharge through several large marine terminating glaciers. Climate
162 change in recent decades have seen substantial thinning of the Tuto dome, shrinking and loss
163 of permanent snowfields across the peninsula, and tidewater glacial retreat of 1–5 km
164 (Copernicus, 2019; Korsgaard et al., 2016; Müller et al., 2021).

165 The Pituffik region holds an outsized role in the ecology and history of the Greenlandic and
166 Canadian High Arctic. Due in part to its proximity to the North Water polynya, Pituffik
167 supports immense seabird colonies in Baffin Bay coastal valleys and hosts important habitat
168 for large populations of marine mammals and waterfowl (Burnham et al., 2014; Hastrup et
169 al., 2018; Heide-Jørgensen et al., 2016; Mosbech et al., 2018). This biological productivity
170 has drawn humans to the region for thousands of years (Gronnow, 2016; Hastrup et al.,
171 2018), and the Thule culture, ancestral to modern Inuit and Greenlandic peoples, was first
172 formally described from excavations conducted on the northern coast of the Pituffik
173 Peninsula (Jenness, 1925). Today, the surface across most of the entire peninsula is covered
174 by coarse glacial deposits with sparse polar desert vegetation (Corbett et al., 2015; Funder,
175 1990; Nichols, 1953). More lush vegetation occurs in low-lying moss wetlands and within the
176 seabird colony valleys (Cuyler et al., 2022; Mosbech et al., 2018) while vast stretches of

177 boulder and cobble outwash plains that extend out from the GrIS margin support only lichens
178 (Davies & Reitzel, 1963).

179 In the 1950s, Pituffik gained global importance and notoriety with the American construction
180 of Thule Air Base (now Pituffik Space Base) as part of the Cold War militarization of the
181 Arctic. Over 10000 American personnel were present for the initial construction and
182 occupation of the base, and at this time these soldiers and contractors comprised over one
183 quarter of the total population of Greenland. Construction of the base ushered in a period of
184 forced relocations of indigenous communities, environmental degradation, and novel
185 resource access that has major ongoing impacts on Greenlandic culture and home rule
186 debates today (Colgan et al., 2016; Eriksson et al., 2004; Gronnow, 2016; Takahashi, 2019).

187 The presence of the military base has also made the Pituffik Peninsula a focal point for
188 environmental studies of the Arctic and cryosphere. American military funding in the early
189 Cold War sent engineers, geologists, and climatologists to Pituffik to test experimental
190 methods of boring into permafrost and the GrIS (Nichols, 1953; Ries, 2012; Schytt, 1955;
191 Swinzow, 1962). While the clandestine goal of ice sheet-spanning tunnel networks to house
192 nuclear weapons failed (Amstrup, 1997; Petersen, 2008; Weiss, 2001), the studies laid much
193 of the foundational research for modern ice core drilling and paleoclimate studies (E. F.
194 Clark, 1965; Dansgaard et al., 1969; Hansen & Langway, 1966). More recently, the logistical
195 ease of transport to the base coupled with housing and entertainment infrastructure has made
196 Pituffik an attractive option for hosting multiyear environmental research projects (e.g.,
197 Akers et al., 2020; Burnham et al., 2014; Corbett et al., 2015; Jespersen et al., 2022; Leffler
198 & Welker, 2013). Our research builds off this extensive foundational knowledge and used the
199 extensive local infrastructure of housing and roads to achieve our dataset's impressive
200 spatiotemporal extent.



201

202 **Figure 1.** Map of the Pituffik region of northwest Greenland. Across the full Pituffik
 203 Peninsula (a), water sample sites (circles) are colored according to the type of surface water
 204 sampled. The eight lake and stream sites frequently sampled for temporal study are shown by
 205 triangle icons. Note that samples for the Pingorsuit and Tuto Forks of the Sioraq River were
 206 both taken at the Fox Canyon Bridge where the forks join. Lakes and pools sampled during
 207 each of the three main sampling periods for interannual analysis are highlighted by pink. The
 208 main lakes region is given additional focus (b) to show the spatial distribution of the main

209 lakes and their lake type categories. Note that no vale or proglacial lakes are present in the
210 main lakes region. Geospatial data used to construct the map includes ArcticDEM (Porter et
211 al., 2019), ice and ocean masks from the Greenland Ice Mapping Project (Howat, 2019), and
212 place names from the Language Secretariat of Greenland (Oqaasileriffik, 2022).

213 **3 Materials and Methods**

214 **3.1 Hydrological survey and geospatial database**

215 We created a new hydrological geospatial database at a previously unavailable resolution and
216 detail for the Pituffik region to support our isotopic field sampling. Field observations of the
217 regional hydrology made during the 2018 and 2019 sampling campaigns provided the
218 foundation and ground-truthing for later geospatial analyses. These analyses and map
219 creations were performed through QGIS with *GRASS*, *GDAL*, *SAGA*, and *Point Sampling*
220 packages. Drainage basins and stream networks for the Pituffik region were extracted from
221 the 2 m ArcticDEM (PGC, 2019; Porter et al., 2019) with *GRASS* flow and drainage tools.
222 Lakes and roads were hand digitized based on both Sentinel 2 satellite imagery from 15
223 August 2019 (Copernicus, 2019) and orthorectified aerial imagery from summer 1985
224 (Korsgaard et al., 2016). Each lake was assigned a lake type category (from the list of
225 endorheic, headwater, downstream, vale, proglacial, and altered) based on its hydrological
226 connectivity and environmental character observed in the field.

227 Geographic coordinates for water sampling sites and notable landmarks were taken with an
228 iPhone 7 GPS and later validated for accuracy with the satellite and aerial imagery.
229 Elevations for sampling sites were extracted from the 2 m ArcticDEM using validated site
230 geographic coordinates. For each lake, the distances to the ocean and to the GrIS (i.e., the
231 Tuto dome margin) were calculated in QGIS as the minimum horizontal distance between the
232 centroid of each lake and the perimeter of the polygons enclosing the ocean and the ice sheet,
233 respectively, using ocean and ice masks defined from the Greenland Ice Mapping Project
234 (GIMP) (Howat, 2019; Howat et al., 2014). Perennial snow patches were excluded from the
235 GIMP ice mask for this calculation to ensure that distances were to the actual GrIS margin.

236 **3.2 Field sampling**

237 Field sampling of Pituffik surface waters occurred when we were present at Pituffik in June–
238 August 2018, November 2018, and July 2019. The samples sort into seven categories based
239 on their source origin: lakes (standing body of water $> 1000 \text{ m}^2$ surface area with a defined
240 shoreline), pools (shallow standing body of water $< 1000 \text{ m}^2$ surface area and/or no defined
241 shoreline), streams (continuous summer flow in a defined channel), surface flow (sheet
242 flow/seeps with undefined channels and also very small intermittent streams), snow or ice
243 (including aged remnant snow patches, remnant lake ice, glacial/multiannual ice, and frost),
244 and both rain and snow precipitation events. We divide the summer sampling into three main
245 periods: early summer 2018 (14 Jun–18 Jul), late summer 2018 (19 Jul–23 Aug), and mid-
246 summer 2019 (19 Jul–01 Aug). Sampling in November 2018 was restricted to precipitation
247 events and the local snowpack as all lakes, streams, and other surface waters were frozen or
248 dry. Aside from the local military road network, no marked trail systems exist in Pituffik, and
249 sample site discovery and access was gained through overland hiking across the tundra and
250 boulder outwash plains to geographic coordinates identified through satellite imagery.

251 Water sampled for isotopes was collected in clean and dry 50 ml plastic centrifuge tubes that
252 were closed tightly and sealed with Parafilm. For lakes and pools, water was sampled 10–20
253 cm below the surface from a downwind shore. For streams, water was collected for 3–10
254 times the duration required to fill the tube ($\sim 5\text{--}30 \text{ s}$). For snow and ice sampling, enough
255 snow or ice was collected to fill the tube whereupon it was sealed and allowed to melt at
256 ambient air temperature. Rain and snow precipitation were sampled as soon as possible after
257 each event ended from accumulation in clean rain gauges or, in the case of some snow events,
258 in bowls or the ground surface outside building 345 on Pituffik Space Base. For all water
259 samples, tubes were filled as full as possible to limit evaporation into the head space and
260 shipped in liquid state for storage and later aliquot sampling. Monthly GNIP precipitation
261 data collected at Thule Airport between 1966 and 1971 (IAEA/WMO, 2022) were
262 downloaded to construct a LMWL for isotopic comparison. Meteorological data for 2018–
263 2019 were collected through weather stations at two sites on the military base (Muscarì,
264 2018; USAF, 2019). Daily potential evapotranspiration (PET) rates for Pituffik were
265 downloaded from a 0.1° spatial resolution dataset modeled with ERA5-Land reanalysis data
266 (Singer et al., 2021).

267 Although most lakes and streams were only sampled once each sampling period due to
268 remoteness, we chose two lakes and six stream sites that were easily accessed by road to
269 frequently sample (i.e., 10–18 times each) (Figure 1). This frequent sampling provided more
270 detailed insight into isotopic evolution of the lakes and streams over time. The sampling of
271 these eight sites in 2018 covered most of the thawed summer season from 14 June through 23
272 August while sampling in 2019 spanned 15 days from 17 July through 01 August. The two
273 frequently sampled lakes, Lake Potato and Power Lake, are located only 1 km apart with
274 similar surface elevations (190 and 178 m a.s.l., respectively) and surface areas (60289 and
275 59537 m², respectively) but belong to different watersheds. Additionally, Lake Potato is the
276 fourth lake in a chain along the Amitsuarsuk River (Potato Creek) and has a large upstream
277 drainage basin of 4.9 km² while Power Lake is a headwater lake with a small 0.3 km²
278 drainage basin and limited outflow. Together, these two lakes are broadly representative in
279 type of most non-proglacial lakes in the Pituffik region.

280 The six frequently sampled stream sites were equally split between the Pituffik River and
281 Sioraq River, which together drain 29% of the ice-free Pituffik region. Both these streams
282 receive meltwater directly from the Tuto dome of the GrIS but also drain wide expanses of
283 tundra and some perennial snow patches. To examine the potential effect of different
284 headwater sources on stream isotopes, we regularly sampled each stream mouth as well as
285 two major upstream forks for each stream: the Ice Wall and Snoutwash Forks for Pituffik
286 River, and the Tuto and Pingorsuit Forks for Sioraq River. The Ice Wall, Snoutwash, and
287 Tuto Forks all originate at different points along the GrIS margin, but the Pingorsuit Fork
288 originates in a permanent montane ice field separate from the GrIS.

289 Stable isotope ratios ($\delta^{18}\text{O}$ and $\delta^2\text{H}$) of 2 ml aliquots were measured at the University of Oulu
290 using a Picarro L2130-i isotope and gas concentration analyzer fitted with an autosampler
291 (A0325) and vaporizer unit (A0211). Reference standards of USGS-45 ($\delta^{18}\text{O}$: -2.2 ‰, $\delta^2\text{H}$:
292 -10.3‰) and USGS-46 ($\delta^{18}\text{O}$: -29.8 ‰, $\delta^2\text{H}$: -235.8 ‰) were used within each analytical
293 run to monitor and correct for instrumental drift as well as to calibrate to the SMOW-SLAP
294 scales for reporting. Each water sample was measured seven times with data from the first
295 three measurements discarded to limit potential memory effects. Samples were reanalyzed if
296 the standard deviation exceeded 0.3 ‰ for $\delta^{18}\text{O}$ or 3 ‰ for $\delta^2\text{H}$, or if the reference standard
297 used in the run differed from the known isotope value by greater than ± 0.2 ‰ for $\delta^{18}\text{O}$ or ± 2
298 ‰ for $\delta^2\text{H}$. These standards span the full isotopic range of our Pituffik water samples except

299 for seven winter snow events and two snowpack samples. Although these snow samples'
300 involvement in further analyses was limited, we are still confident of their values as the
301 calibrated Picarro instrument linearly infers isotopic ratios to values well below any of our
302 samples (Casado et al., 2016). Based on within-run replicate analyses of standard waters,
303 mean analytical precision was ± 0.1 ‰ for $\delta^{18}\text{O}$ and ± 0.6 ‰ for $\delta^2\text{H}$. Eighteen water samples
304 were flagged during quality control for having visibly cracked and/or leaking vials after
305 transport, and these samples, along with two tap water samples taken on Pituffik Space Base,
306 were not included in further analyses.

307 **3.3 Spatial and temporal analyses**

308 Beyond a basic overview of all surface water isotopic variability across the Pituffik
309 landscape, we focused our study on the spatial and temporal variability of lake and stream
310 isotopic compositions. Because the isotopic composition of non-frozen surface waters is
311 constantly evolving in response to changes in precipitation, runoff, and evaporation (Gibson
312 et al., 1998; Gibson & Reid, 2014), any attempt to compare water isotopes spatially across
313 multiple lakes and/or streams requires that the water samples are all collected in as short of a
314 time window as possible. Our spatial study of lake isotopic compositions therefore focused
315 on 63 lakes sampled during the two-week period in mid-summer 2019 because this dataset
316 represents nearly all Pituffik lakes while also having a short sampling period that limits
317 temporal isotopic impacts.

318 The spatial analysis first focused on whether lake type categories assigned to each lake have a
319 relationship with lake isotopic compositions based on isotopic distributions per lake type
320 category and hierarchical cluster analysis of lake $\delta^{18}\text{O}$ and d_{xs} values. Following the lake
321 type results, we performed multiple regression and LASSO regression between the three
322 isotopic variables and six lake parameters of surface elevation, surface area, watershed area,
323 distance from nearest GrIS margin, distance from nearest ocean coast, and day of year
324 sampled. We restricted this analysis further from the lake type analysis dataset to include
325 only 42 headwater and downstream lakes located in the main lakes region. By narrowing our
326 analysis to this subset of lakes that share common hydrological settings and similar isotopic
327 compositions, the subtle influences of lake parameters could emerge beyond the wide
328 isotopic differences that span lake type categories. Our study on the spatial variability of

329 streams was more limited and focused on comparing the isotopic composition of samples
330 from the three stream networks of the Pituffik, Sioraq, and Amitsuarsuk Rivers.

331 The temporal analysis of lake isotopes examined isotopic evolution over the 2018 summer
332 season as well as between the summers of 2018 and 2019. For these analyses, we used both
333 the frequently sampled Lake Potato and Power Lake data and a multi-annual subset of 18
334 lakes and 2 pools that were sampled for water isotopes during each of the three main
335 sampling periods. Finally, we also examined the temporal variability of stream water isotopes
336 using the frequently sampled data from three sites each on the Pituffik and Sioraq Rivers.
337 Both lake and stream isotopic changes over time were compared with local weather records
338 (Muscari, 2018; USAF, 2019) and modeled PET (Singer et al., 2021) to interpret the roles of
339 key climatological parameters might play in the observed isotopic changes over time.

340 Statistical analyses and figure creation were performed in RStudio using the R language with
341 packages *ape*, *broom*, *clock*, *cowplot*, *dendextend*, *gridExtra*, *ggdendro*, *glmnet*,
342 *gridgraphics*, *ncdf4*, *raster*, *reshape2*, *Rmisc*, and *tidyverse*, and figures were aesthetically
343 adjusted in Adobe Illustrator. Uncertainties for statistical values are given as 95% confidence
344 intervals unless otherwise noted.

345

346 **4 Results**

347 **4.1 Hydrological survey and geospatial database**

348 The geospatial data resulting from our hydrological survey has been made openly available as
349 a geospatial database (Akers et al., 2023b). Individual vector files in the database include
350 points of field observations and placenames, polylines of elevation contours, roads, stream
351 networks, and drainage divides, and polygons for lakes, lake drainage basins, stream drainage
352 basins, ice-covered land, and ice-free land. Raster data of digital elevation models (PGC,
353 2019), aerial imagery (Korsgaard et al., 2016), and satellite imagery (Copernicus, 2019) for
354 the Pituffik region is not provided in the geospatial database due to large file sizes, but can be
355 downloaded from their original, openly available sources. Using the geospatial database, we
356 created a hydrology and surface features map for Pituffik that is offered as both a large poster

357 (Figure S1) and as a multipage atlas (Akers et al., 2023b). A general overview of the Pituffik
358 surface water landscape as informed by our hydrological survey results follows.

359 The surface drainage system of the peninsula is dominated by four main river and stream
360 networks (hereafter referred to collectively as streams) that each drain over 100 km².
361 Together, these four basins of the Sioraq (South River), Paakitsoq (Pituffik Glacier River),
362 Pituffik (North River), and Narsaarsuk Rivers cover half of the non-glaciated land surface of
363 the Pituffik region. An additional six streams (Maniiseqqat, Illuluarsunnguit, Quaraatit,
364 Nipitartooq, Qoororsuaq, Iterlak, and Amitsuarsuk Rivers) drain basins each larger than 10
365 km² while numerous smaller basins directly drain coastal lands into the ocean. Of the ten
366 largest stream basins, only three directly drain meltwater from the GrIS: the Pituffik River,
367 Sioraq River, and Paakitsoq River. Outside of the larger streams, well-defined channels are
368 rare across the landscape with most local drainage occurring as sheet flow across the surface
369 or subsurface flow through the coarse rocky active layer.

370 The Pituffik hydrological system is highly reactive to the thaw of waters frozen in snowpack,
371 glacial ice, and surface waters brought on by both typical seasonal warming and irregular
372 short-term heat events. Although Pituffik surface waters are dry and/or frozen for 7–8 months
373 of the year, the melting of the winter snow cover in May–June (Figure S2) brings an initial
374 period of high surface flow and numerous small pools left in depressions across the tundra.
375 These pools drain in 2–3 weeks as summer progresses and the active layer deepens, and
376 summer flows for streams not sourced at the GrIS are sustained largely by melting residual
377 snow patches (Figure S3). For the three stream basins linked to the GrIS, water discharge
378 often exhibits two seasonal peaks (Csank et al., 2019). After the initial early summer pulse
379 from the melting of the winter tundra snowpack, streamflows also increase in later summer as
380 a result of surface melting of the GrIS and its snow cover. During extreme heat events, such
381 as in 2012 and 2019 (Cullather et al., 2020; Nghiem et al., 2012; Sasgen et al., 2020), massive
382 volumes of glacial runoff greatly swell the streams sourced at the GrIS and can threaten local
383 infrastructure (Figure S3b, d).

384 The Pituffik region also hosts numerous permanent lakes and ponds (hereafter referred to
385 collectively as lakes) typically formed in Late Pleistocene moraines and till (Figure S4).
386 Around 70 non-proglacial lakes across the peninsula have a surface area greater than 5000
387 m², and several very large proglacial and ice-dammed lakes occur along the margins of the
388 Tuto ice dome and its outlet glaciers. In total, approximately 3.8 km² of the Pituffik surface is

389 covered by lakes, of which 2.4 km² are non-proglacial. These lakes are typically frozen over
390 between September and April, with ice-out beginning in late May to early June (Figure S2,
391 Figure S5). For the largest lakes, ice cover is largely intact through June, and some ice may
392 remain even into August in colder summers. Over half of the region's lakes are clustered in a
393 23 km² zone north of Pituffik River and northeast of the military base which we refer to as
394 the "main lakes region" (Figure 1b). The construction of military buildings and roads have
395 affected some surface drainage and lakes, most notably with the conversion of Lake Crescent
396 into a dammed reservoir (Davis, 1966), but aerial photographs (Figure S6) predating the
397 base's construction show that the vast majority of lakes still retain their natural layout
398 (Historiske Kort, 2023). We could not find indigenous names for Pituffik lakes despite
399 extensive efforts, and only a few lakes have local English or Danish names. We therefore
400 informally assigned most of the lake names in our database.

401 Across the Pituffik region, we sorted lakes into six lake type categories based on each lake's
402 environmental and hydrological setting: endorheic, headwater, downstream, vale, proglacial,
403 and altered (Figure 1b, Figure 2, Figure S4). We assigned these lake types prior to any
404 isotopic analysis based solely on physical lake characteristics observed during field sampling.
405 Endorheic lakes fill the low points of small enclosed basins with ill-defined shorelines and
406 have no clear inflow or outflow channels, although it is possible that some subsurface water
407 exchange occurs in the active layer above the permafrost. A headwater lake is connected to a
408 fluvial network but has no lake farther upstream, whereas a downstream lake is any lake
409 along a fluvial network that receives upstream water from at least one other lake. Lake fluvial
410 interconnections may be through stream channels or less defined surface and near-surface
411 flow, and blanketing moss is typically extensive along the shores of headwater and
412 downstream lakes and along their connecting drainage routes. Vale lakes are found within
413 rocky steep-sided valleys primarily located south of Pituffik Space Base. Although vale lakes
414 are interconnected by valley drainage systems, they differ from headwater and downstream
415 lakes in their lack of clear shorelines, near absence of any surrounding vegetation, and rugged
416 topographic setting. The proglacial lakes sampled in our study form a connected chain
417 directly in contact with the GrIS margin that are fed by melting glacial runoff and eventually
418 drain into the Sioraq River. Altered lakes either exist only because infrastructure has blocked
419 natural drainage or are natural lakes whose watershed and drainage are so heavily disrupted
420 by human changes that they no longer reflect natural conditions. We assigned one lake type
421 category to each lake based on observations in the field, but we emphasize that these

422 categorizations were personal judgments to sort lakes that may fall along a continuum of
423 types.

Examples of Pituffik lake types



a) Endorheic: Angry Duck Lake



b) Headwater: Carex Pond



c) Downstream: Lake Tre



d) Vale: Rocky Vale Lake



e) Proglacial: Iceberg Lake



f) Altered: Gravel Pit Lake

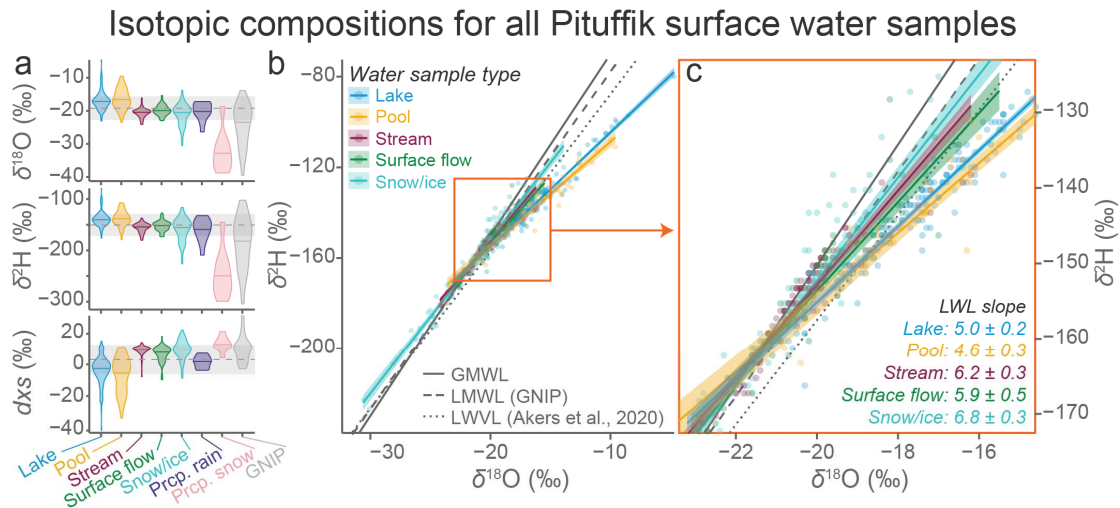
424

425 **Figure 2.** Photographic examples of the six lake type categories assigned to Pituffik lakes.
426 Each lake example here exhibits the major defining characters of its lake type. Note in
427 particular (a) the shallow depth and ill-defined shoreline of the endorheic Angry Duck Lake,
428 (b) the vegetated shoreline hydrologically constraining the headwater Carex Pond, (c) the
429 Amitsuarsuk River flowing through the downstream Lake Tre, (d) the lack of vegetation and
430 steep valley (i.e., vale) setting of Rocky Vale Lake, (e) the direct contact of proglacial
431 Iceberg Lake with the GrIS margin, and (f) the exposed former lake bed of altered Gravel Pit
432 Lake which was partially drained through an artificial outlet channel.

433 **4.2 General isotopic summary**

434 In total, we collected 535 samples from 196 unique sites across the Pituffik region,
 435 representing 67 lakes, 37 pools, 24 sites along major streams, 50 sites with surface flow, and
 436 57 snow or ice deposits. The $\delta^{18}\text{O}$, $\delta^2\text{H}$, and dxs of the samples largely fall within similar
 437 ranges regardless of origin type with mean $\pm 1\sigma$ isotopic values for all samples of $\delta^{18}\text{O}$:
 438 -19.3 ± 3.6 ‰, $\delta^2\text{H}$: -151 ± 22 ‰, and dxs : $+3 \pm 9$ ‰ (Figure 3a). The isotopically much
 439 lighter winter snow precipitation events are an exception to this general similarity. Across the
 440 other samples, we observe that lake and pool are generally isotopically heavier than other
 441 sample types, while the dxs of lakes and pools are on average lower than other types with a
 442 substantial skew towards extreme lower values of -10 to -40 ‰. This wide range in Pituffik
 443 lake isotopic values is comparable in magnitude to the isotopic range reported from lakes
 444 1300 km south in Kangerlussuaq, Greenland (Cluett & Thomas, 2020; Leng & Anderson,
 445 2003). The mean $\delta^{18}\text{O}$ and $\delta^2\text{H}$ values of streams, surface flow, and snow/ice deposits are
 446 similar to our observed rain events and much higher than snow events, but their dxs values
 447 are intermediate between rain and snow events.

448



449

450 **Figure 3.** Isotopic compositions of Pituffik surface waters. Violin plots (a) show the
 451 distributions of isotopic ratios of Pituffik water samples, grouped by sample source type.
 452 Data are plotted so that the maximum width is equivalent between groups, regardless of
 453 sample count. The mean isotopic values ± 1 standard deviation of all water samples are
 454 shown by the dashed line and gray shaded bar crossing all violins. Within each violin, the

455 median value per group is shown by a solid horizontal line. GNIP samples are monthly
456 precipitation means collected between 1966 and 1971 (IAEA/WMO, 2022). In (b), linear
457 regressions between $\delta^{18}\text{O}$ and $\delta^2\text{H}$ illustrating local water lines (LWLs) are shown for the
458 different sample source types with shading representing the 95% confidence interval of the
459 regression. The global meteoric water line (GMWL, solid gray), local meteoric water line
460 (LMWL, dashed gray) based on GNIP data (IAEA/WMO, 2022), and local water vapor line
461 (LWVL, dotted gray) (Akers et al., 2020) are shown for reference. The plot in (c) is a
462 magnified version of the area indicated with the orange square in (b), and LWL slope values
463 with 95% confidence intervals are provided for each sample type at lower right. Regressions
464 for precipitation data are provided in Figure S7.

465 Linear regressions of $\delta^2\text{H}$ vs. $\delta^{18}\text{O}$ (the local water lines, or LWLs) show that different water
466 source types isotopically diverge from the GMWL and the LMWL to different degrees
467 (Figure 3b–c, Table S1). Precipitation events of both snow and rain as well as snow and ice
468 sampled from across the landscape have slopes that are similar to the isotopic reference lines
469 (Figure 3, Figure S7). This similarity is expected for the snow precipitation events and
470 surface snow/ice since they are frozen and therefore have not experienced post-precipitation
471 evaporation. Interestingly, while the slope of the summer rain events is within uncertainty to
472 the LMWL, the rain events have a $\approx +5\%$ $\delta^{18}\text{O}$ bias relative to the LMWL (Figure S7). With
473 the limited number of sampled events ($n=14$), it is not fully clear what is causing this bias.
474 Differences in moisture transport and sourcing due to climate change since the GNIP
475 sampling era may partly explain the offset. Additionally, this bias may also result from minor
476 evaporation occurring during the rain events (as the rain falls through an unsaturated lower
477 atmosphere) or in the rain gauge/bowl before collection.

478 In contrast, the liquid surface waters of Pituffik all display some degree of isotopic change
479 from evaporation as evidenced by their lower LWL slopes that we interpret as LELs (Figure
480 3, Table S1). Lakes and pools diverge the most from the LMWL while streams and surface
481 flows diverge less but still noticeably. Theoretically, the intersection of an LEL and the
482 LMWL defines the isotopic values of the initial source water prior to evaporation (Welhan &
483 Fritz, 1977), although this approach has known flaws when the LELs are defined by samples
484 from multiple sources that likely do not share identical initial water isotopic values (Bowen et
485 al., 2018). Acknowledging these limitations, we note that the LELs for lakes, pools, streams,
486 and surface flow all predict very similar initial water isotopic values between -20.0 and

487 -21.0 ‰ for $\delta^{18}\text{O}$ and -153 and -160 ‰ for $\delta^2\text{H}$. These values are slightly higher than the
 488 amount-weighted GNIP mean values of -22.5 ‰ and -173 ‰, which could suggest that the
 489 surface waters are slightly biased toward summer precipitation. However, we also note that
 490 conclusive comparisons are difficult as the Thule GNIP data has several missing months of
 491 isotope data, and mean isotopic values for precipitation today may be higher than during
 492 GNIP's 1966–1971 collection period due to climate change.

493 Building off this foundation of Pituffik surface water isotopic compositions, we focused on
 494 examining the drivers of isotopic variability in the lake and stream samples across both space
 495 and time. We used the pool, surface flow, snow/ice, and precipitation data for environmental
 496 context when interpreting the lake and stream isotopes, but deeper examination of their
 497 isotopic variability is not discussed here. Those interested in these non-lake and non-stream
 498 data are directed to our open access database (Akers et al., 2023a).

499 **5 Isotopic variability in lakes**

500 The isotopic composition of a lake at a given point in time reflects its current isotope-mass
 501 balance (Gibson et al., 2016; Gonfiantini, 1986), represented as

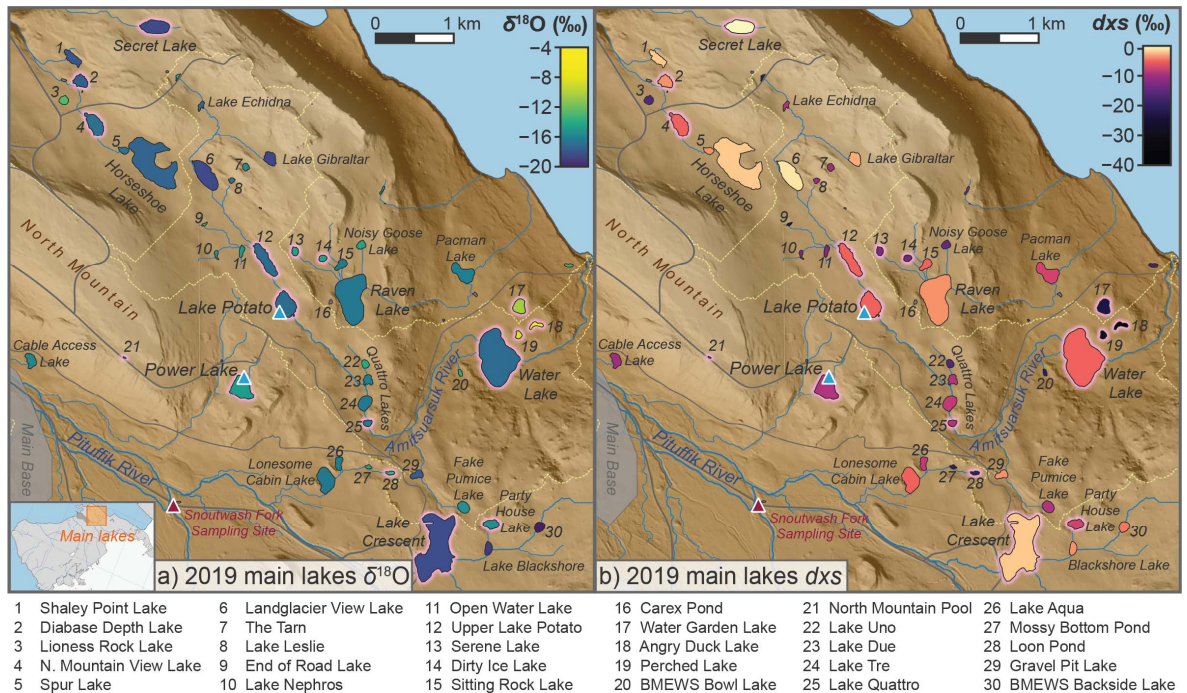
$$502 \quad V \frac{d\delta_L}{dt} + \delta_L \frac{dV}{dt} = I\delta_I - Q\delta_Q - E\delta_E \text{ (‰} \cdot \text{m}^3 \cdot \text{year)} \quad (1)$$

503 where V is the lake volume, t is time, I is total lake inflow, Q is total lake outflow, E is
 504 evaporation, and δ_L , δ_I , δ_Q , and δ_E are the respective isotopic compositions of the lake, inflow,
 505 outflow, and evaporation flux. Based on Eq. 1, we expect lakes with different environmental
 506 characteristics related to volume, inflow, outflow, and evaporation to exhibit spatial isotopic
 507 variability. Likewise, local weather and seasonal climate changes that affect these
 508 hydrological parameters will drive temporal lake isotopic variability. Following this
 509 understanding, we investigated which environmental parameters best explained the observed
 510 spatiotemporal variability in lake isotopes across Pituffik using our large set of lake water
 511 samples.

512 The full set of 67 lakes included in our isotopic dataset represents a near-comprehensive
 513 sampling of total lake variability on the Pituffik Peninsula (Figure 1). These lakes range in
 514 surface area from 1100 – 2000 m^2 for smaller ponds to nearly $260,000$ m^2 for Lake Crescent,
 515 the largest non-proglacial lake in our set and on the peninsula. The lakes are distributed

516 across much of the environmental gradient that follows the elevation rise from the lowest
 517 coastal lakes at 22 m a.s.l. to the highest lakes at 500 m a.s.l near a margin of the GrIS. The
 518 distance to each lake from the ocean varies between 0.07–17.8 km while the distance from
 519 the nearest margin of the GrIS varies between 0.0–16.9 km.

520 The isotopic compositions of Pituffik lakes vary widely across both space and time (Figure
 521 3a, Figure 4). The highest lake $\delta^{18}\text{O}$ and $\delta^2\text{H}$ values of -4.7‰ and -80‰ , respectively, were
 522 observed in the endorheic Angry Duck Lake on 26 July 2019, and this same sampling also
 523 produced the lowest observed d_{xs} value of -42‰ . In contrast, the lowest $\delta^{18}\text{O}$ and $\delta^2\text{H}$
 524 values of -23.2 and $\text{‰} -177$, respectively, were observed in Half Snow Lake, a small lake
 525 abutting a permanent snow patch that is located in the vast boulder outwash plains fronting
 526 the GrIS south of the main lakes region. Many of the proglacial lakes near the Tuto Ice Ramp
 527 have similarly low isotopic ratios as Half Snow Lake, and one of these lakes (Ice Ramp Base
 528 Pond) returned the highest observed d_{xs} value of $+15\text{‰}$ on 7 July 2018. Despite this wide
 529 overall range, most lake samples fall within a much more limited isotopic range (25–75%
 530 quantile ranges: $\delta^{18}\text{O} = -18.6$ to -15.9‰ , $\delta^2\text{H} = -148$ to -134‰ , $d_{\text{xs}} = -7$ to $+1\text{‰}$).



531

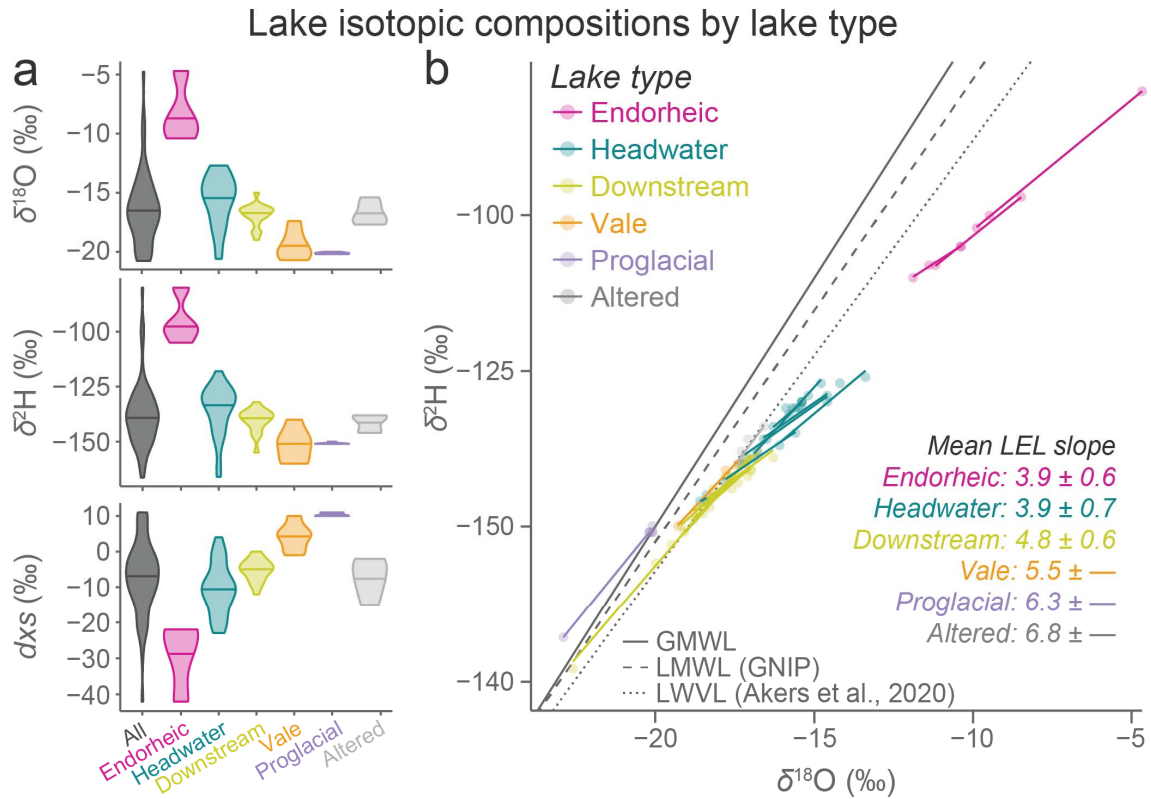
532 **Figure 4.** Water isotopic compositions of lakes sampled in mid-summer 2019 in the main
 533 Pituffik lakes region. Lakes are colored according to their measured $\delta^{18}\text{O}$ (a) and d_{xs} (b)
 534 values. Although $\delta^2\text{H}$ values are not shown here, their relative spatial distribution appears

535 extremely similar to the $\delta^{18}\text{O}$ values (a). Broader regional context, minor isotope identification,
536 and geospatial data sources can be found in Figure 1.

537 **5.1 Spatial variability in lake isotopic composition**

538 **5.1.1 Lake types**

539 In order to minimize any analytical muddling from temporal isotopic evolution (L. Anderson
540 et al., 2013; Arp et al., 2015; Cluett & Thomas, 2020; Gibson & Reid, 2014), we focused our
541 spatial analysis of lake isotopic composition on water samples from 63 lakes that were
542 collected in the two-week mid-summer 2019 sampling period. These 63 lakes were classified
543 by lake type into 26 headwater, 17 downstream, 4 endorheic, 6 vale, 5 proglacial, and 5
544 altered lakes. The isotopic compositions of the different lake types during this period are
545 generally well-grouped and distinct from each other (Figure 5a). The endorheic lakes are the
546 most distinct with $\delta^{18}\text{O}$ and $\delta^2\text{H}$ values much higher than all other lakes and d_{xs} values as
547 low or lower than all other lakes. At the other extreme from the endorheic lakes, proglacial
548 lakes have d_{xs} values higher than all other lakes as well as some of the lowest $\delta^{18}\text{O}$ and $\delta^2\text{H}$
549 values. Headwater and downstream lakes have intermediate isotopic values, although the
550 isotopic range for headwater lakes is much larger and completely overlaps the range in
551 downstream lakes, which can be expected as every downstream lake is connected to at least
552 one headwater lake. Additionally, headwater lakes as a whole have higher mean $\delta^{18}\text{O}$ and
553 $\delta^2\text{H}$ values and lower mean d_{xs} values than downstream lakes. Vale lakes bridge the isotopic
554 value gap between headwater/downstream lakes and proglacial lakes, and altered lake
555 isotopic compositions are similar to headwater and downstream lakes. Although this isotopic
556 similarity suggests that human disruptions have not dramatically changed the hydrology of
557 the altered lakes from what might be naturally expected, we exclude these lakes from
558 subsequent analyses out of caution.



559

560 **Figure 5.** Isotopic composition of lakes sampled across Pituffik grouped by lake type
 561 category. In (a), violin plots show the isotopic composition distribution of all lakes sampled
 562 in 2019 (black) as well as split by lake type (colored). Data are plotted so that the maximum
 563 width is equivalent between groups, regardless of sample count. Within each violin, the
 564 median value per group is shown by a solid horizontal line. In (b), $\delta^2\text{H}$ vs. $\delta^{18}\text{O}$ is plotted to
 565 show local evaporation lines (LELs) for every lake that was sampled at least three times
 566 across 2018 and 2019. Each LEL represents a single lake or pool, and the LELs are colored
 567 according to lake type. The mean and 95% confidence interval of LEL slope values are
 568 displayed per lake type at lower right. Note that the vale and altered lake slopes have no
 569 confidence interval as there is only one lake per type that was sampled at least three times.
 570 Note also that the proglacial lakes do not display a true LEL as the values do not fall below
 571 the LMWL in $\delta^{18}\text{O}$ – $\delta^2\text{H}$ space. The global meteoric water line (GMWL, solid gray), local
 572 meteoric water line (LMWL, dashed gray) based on GNIP data (IAEA/WMO, 2022), and
 573 local water vapor line (LWVL, dotted gray) (Akers et al., 2020) are shown for reference.

574 The LELs of individual lakes suggest that evaporation is a key driver of the isotopic
 575 differences between lake types (Figure 5b). Examining lakes that were sampled at least three

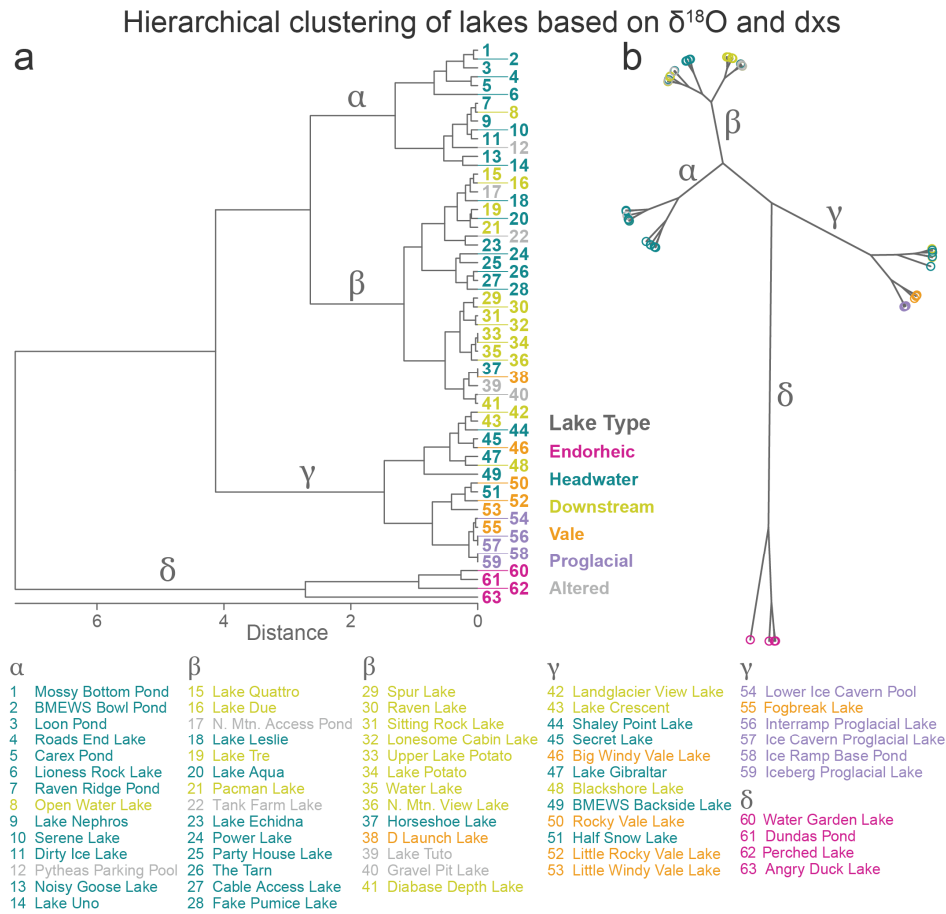
576 times across 2018 and 2019 (number of lakes per type: endorheic = 3, headwater = 7,
 577 downstream = 3, vale = 1, proglacial = 2, altered = 1), we observe that lakes and lake types
 578 with isotopically heavier waters have LELs with lower slopes. This observation suggests that
 579 these isotopically heavier lakes exist in more arid environments that promote lake water
 580 evaporation. This dominance of evaporation agrees with isotopic results from lake systems
 581 elsewhere in Greenland (Kopec et al., 2018; Leng & Anderson, 2003) and in boreal Canada
 582 (Gibson, 2002; Gibson & Reid, 2014) and is notably greater than reported for subarctic lakes
 583 in Sweden (Jonsson et al., 2009).

584 The mean lake LEL slope value differs depending on the method of calculation, and this
 585 difference is important when comparing LEL slopes across studies. The LEL slope calculated
 586 from combining all the lake data, as reported in many other relevant studies (Gibson &
 587 Edwards, 2002; Kopec et al., 2018; Leng & Anderson, 2003; Stansell et al., 2017), is 5.1 ± 0.1 .
 588 This slope is lower than reported for coastal lakes in central West Greenland and Arctic
 589 Alaska (Leng & Anderson, 2003; MacDonald et al., 2017) but higher than more inland lakes
 590 in central West Greenland and the Canadian Arctic (Gibson & Edwards, 2002; Kopec et al.,
 591 2018; Leng & Anderson, 2003). The intermediate slope values for Pituffik suggest that the
 592 arid High Arctic summer coupled with the proximity to the GrIS and its drying katabatic
 593 winds promote a more evaporative environment than might be expected for its coastal
 594 location. However, if the LELs are calculated individually for lakes and then averaged, the
 595 mean slope value is 4.6 ± 0.5 . Few Arctic studies report lake LELs based on this method for
 596 comparison, but our observed slope difference highlights the flawed assumption of identical
 597 initial water isotopic compositions made when aggregating all regional lakes into a single
 598 LEL (Bowen et al., 2018; MacDonald et al., 2017).

599 Indeed, the intersections between individual Pituffik lake LELs and the LMWL suggest that
 600 the initial isotopic composition of lakes differs by lake type. The sampled proglacial lakes do
 601 not produce an LEL, suggesting that their waters have not experienced substantial
 602 evaporative loss and that their observed isotopic composition is their initial isotopic
 603 composition. This is logical as the proglacial lakes are directly in contact with and supplied
 604 by the melting of the GrIS. For the other lake types, the mean predicted initial isotopic
 605 composition is the heaviest for endorheic lakes ($\delta^{18}\text{O} = -17.1 \pm 0.9 \text{‰}$, $\delta^2\text{H} = -131 \pm 7 \text{‰}$)
 606 followed by headwater lakes ($\delta^{18}\text{O} = -19.7 \pm 0.8 \text{‰}$, $\delta^2\text{H} = -150 \pm 6 \text{‰}$), downstream lakes
 607 ($\delta^{18}\text{O} = -20.9 \pm 0.8 \text{‰}$, $\delta^2\text{H} = -159 \pm 6 \text{‰}$), and then vale lakes ($\delta^{18}\text{O} = -20.6 \text{‰}$, $\delta^2\text{H} = -157$

608 %, based on single LEL). The isotopically heavier initial values predicted for endorheic and
 609 headwater lakes suggest that these lakes are sourcing relatively more warm season
 610 precipitation versus isotopically light winter snowpack, perhaps due to their smaller and more
 611 isolated watersheds that limits their supply from tundra-wide snowpack melt.

612 Hierarchical clustering based on the lake water $\delta^{18}\text{O}$ and d_{xs} values (Figure 6a–b) sorts the
 613 lakes in four main clades and supports our lake type categorization as reflecting real
 614 differences in lake hydrology. Although the lake types are not perfectly sorted into the clades,
 615 the clades resulting from the hierarchical clustering are better explained by lake type category
 616 than by specific lake parameters such as size, elevation, or particular watershed. This argues
 617 that lake isotopic composition is strongly influenced by hydrological connectivity, which is
 618 central to lake type character and categorization.



619

620 **Figure 6.** Hierarchical clustering results for Pituffik lakes based on $\delta^{18}\text{O}$ and d_{xs} values.
 621 Results are shown in two forms of dendrogram (a, b) with individual lakes colored according

622 to lake type. Four prominent clades are identified with Greek letters. Lake names referencing
623 the numerical results in (b) are provided at bottom.

624 The four endorheic lakes comprise their own clade (δ) well-separated from all other lakes,
625 validating the isotopic distinctiveness of this lake type. The extreme isotopic values and
626 distinct clade identity of the endorheic lakes reflect evaporation's dominance of their water
627 balance as supported by their shared lowest mean LEL slope values (Figure 5b). Angry Duck
628 Lake, the lake whose 2019 water sample had the heaviest isotopic composition and lowest
629 δx_s values of all lake samples, is a very shallow endorheic lake whose size changes year to
630 year reflecting water balance. In fact, many of the Pituffik endorheic lakes have severely
631 shrunk in size or even disappeared since 2020. Similarly low endorheic lake levels observed
632 in 2016 (Copernicus, 2019) and 1949 (Figure S6) suggest that the loss of these endorheic
633 lakes is not a recent phenomenon due to climate change, but rather that they are simply
634 highly sensitive to short-term water balance changes. These endorheic lakes function
635 similarly to idealized evaporation pans due to their lack of channel outflow, permafrost that
636 blocks groundwater inflow and outflow, and small, self-contained basins that limit input from
637 precipitation. The low mean LEL slope value and isotopically heavy initial water values for
638 endorheic lakes (Figure 5b) reflect a consistently arid environment whose lake waters are
639 perhaps more sensitive to and reflective of isotopically heavier summer precipitation.

640 Headwater and downstream lakes have similar isotopic values, but the LELs and cluster
641 analysis support that they have detectable hydrological differences. The lower LEL slope
642 values, higher mean $\delta^{18}\text{O}$ and $\delta^2\text{H}$ values, and lower mean δx_s values of headwater lakes
643 suggests that they have on average greater evaporation losses than downstream lakes (Figure
644 5a–b). This may seem counterintuitive at first because downstream lakes receive water that
645 has already experienced isotopic change from evaporation in upstream lakes, and additional
646 evaporation in a downstream lake should only add to the existing isotopic changes. However,
647 headwater lakes have a smaller surface area on average than downstream lakes (mean \pm 95%
648 confidence interval: $20950 \pm 16230 \text{ m}^2$ vs. $65290 \pm 38560 \text{ m}^2$, respectively), and heavier
649 isotope enrichment in smaller lakes due to greater relative evaporation loss has been
650 previously reported for Greenlandic lakes (Kopec et al., 2018). Assuming that surface area is
651 correlated with volume, the smaller volume of headwater lakes would enhance the relative
652 evaporation component of the headwater lake water balance, and their smaller watersheds
653 also limit the amount of precipitation input from runoff. Many of the smaller headwater lakes

654 are shallow enough to freeze to their beds in winter, resulting in earlier spring ice melt and
655 greater potential summer evaporative loss (Arp et al., 2015). Additionally, these headwater
656 lakes likely only supply a minor component of the overall water input to downstream lakes
657 relative to total basin runoff, and thus their evaporation-altered water does not likely not
658 provide substantial input by volume to downstream lakes.

659 Indeed, one clade identified in the cluster analysis (α) almost entirely contains headwater
660 lakes, and closer investigation of this clade's lakes reveals that they are all particularly small
661 lakes (surface area mean \pm 95% CI = 5750 ± 1630 m²) without stream channel connections to
662 their larger watersheds. Clear downstream drainage does occur from these lakes, but their
663 drainage routes and shores are thickly vegetated in moss which slows outflow and
664 hydrologically isolates the lakes. The largest clade (β) contains a mix of headwater and
665 downstream lakes that are generally larger in surface area and better hydrologically
666 connected than the α -clade. Notably, nearly half of all downstream lakes are exclusively
667 clustered in a single subgroup of this clade despite belonging to four different watersheds,
668 suggesting that their downstream nature is a stronger determinant of isotopic composition
669 than their particular hydrologic basin.

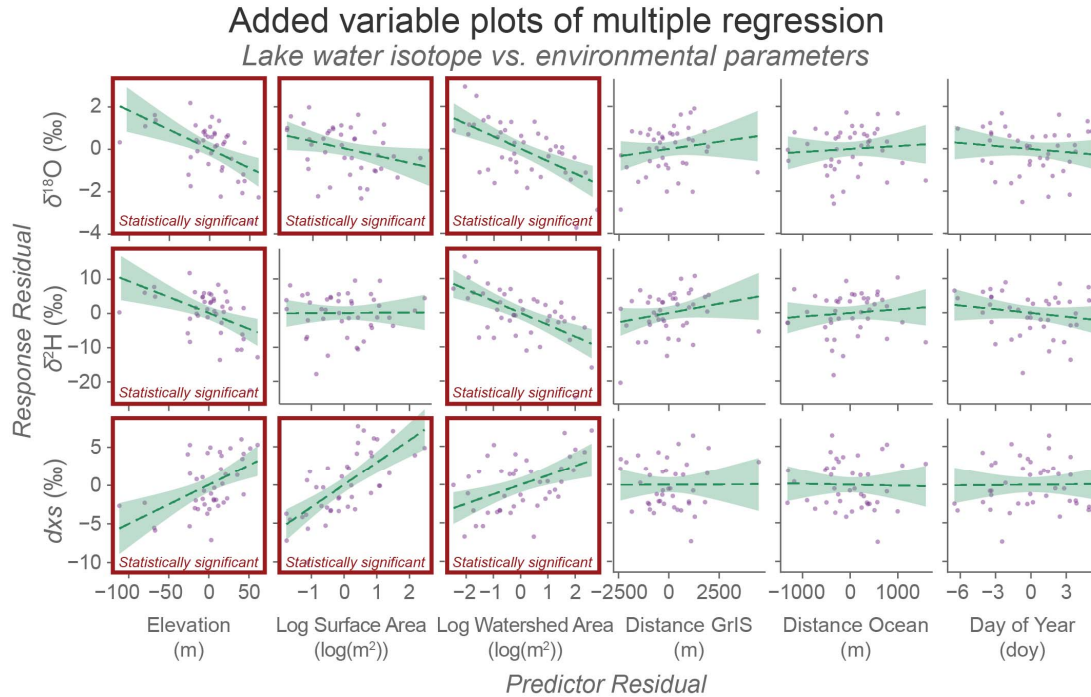
670 Finally, the remaining clade (γ) initially appears to be a confusing mix of headwater,
671 downstream, vale, and proglacial lakes. However, these lakes mostly share a rocky rather
672 than vegetated shore and a direct hydrologic connection to ice and snow patches that linger
673 long past the early summer melt of the general tundra snowpack. The proglacial lakes
674 comprise one distinct subgroup of this clade along with a vale lake (Fogbreak Lake) that is
675 hydrologically similar to a proglacial lake as it has only recently formed as a large permanent
676 snow patch partially retreated. Proglacial and vale lakes have isotopic values very similar to
677 the mean value of Pituffik snow and ice samples (Figure 3) which reflects their summer-long
678 recharge from the melting of permanent snow from the GrIS or patches shaded by the steep
679 vale valley slopes.

680 The headwater and downstream lakes in the γ -clade generally have watersheds that drain
681 substantial high altitude areas, and the continuing late season snowmelt supply pushes the
682 isotopic character of these lakes closer to proglacial and vale lakes. For example, Half Snow
683 Lake is classified as a headwater lake based on its hydrological setting, but it provided the
684 isotopically lightest lake water sample in our dataset and falls within the γ clade. As its name
685 suggests, Half Snow Lake abuts a large permanent snow patch, and this snow patch provides

686 a steady supply of isotopically light meltwater to Half Snow Lake over the summer in a
687 manner hydrologically similar to the proglacial lakes. Overall, it is important to note that
688 while each lake type can be said to have a typical isotopic and environmental character, the
689 lake type categories do not have hard boundaries, and several lakes are clearly hybrid or
690 transitional lake types. Additionally, hydrological factors specific to each lake other than the
691 simple lake type category (e.g., presence of local snow patches, depth and thermal
692 stratification, etc.) can skew individual lakes away from what would be expected based solely
693 on the mean isotopic values of their lake type.

694 **5.1.2 Hydrological parameters**

695 Lake type sets the general value expected in a lake's isotopic composition, but other
696 environmental parameters influence the isotopic composition of Pituffik lakes within each
697 lake type group. To examine these parameters, we performed multiple regression and LASSO
698 regressions on the subset of 42 headwater and downstream lakes sampled in mid-summer
699 2019 from the main lakes region (Figure 1b, Figure 4). Both multiple and LASSO regressions
700 identified elevation, surface area, and watershed area as having important influences on lake
701 isotopic composition, but their relative importance differed depending on specific isotopic
702 variable (Figure 7, Table S2). Both lake surface area and watershed area are known as key
703 components of lake water balance in the Arctic (e.g., Gibson & Reid, 2014; Wilcox et al.,
704 2023), and it is thus not surprising that they emerged as strong environmental drivers at
705 Pituffik. Day of year sampled and the distances from the GrIS and ocean did not have notable
706 relationships with isotopes. This is in contrast to prior studies in Søndre Strømfjord,
707 Greenland (Kopeck et al., 2018; Leng & Anderson, 2003), and northern Scandinavia
708 (Kjellman et al., 2022) that detected clear relationships between lake isotopic composition
709 and distance from the ocean. However, both these studies examined lakes on much longer
710 transects away from the coast (150–460 km) than available at Pituffik (<20 km), and it is
711 probable that the distance from the ocean simply is not large enough at Pituffik to emerge as
712 a primary driver of isotopic variability.



713

714 **Figure 7.** Added variable (i.e., partial regression) plots of the multiple regression of each lake
 715 isotopic variable versus six environmental parameters. Regressions are shown as green
 716 dashed lines with 95% confidence intervals of the regression shown in green shading. Lake
 717 samples included in the multiple regressions were restricted to headwater and downstream
 718 lakes sampled in mid-summer 2019 from the main lakes region north of the air base.
 719 Parameters that produced statistically significant multiple regression coefficients for specific
 720 isotopic variables (Table S2) are outlined by red boxes.

721 The $\delta^{18}\text{O}$ and $\delta^2\text{H}$ share similar influential parameters on lake isotopic composition (Figure 7,
 722 Table S2). For $\delta^{18}\text{O}$, the most influential parameter is the lake watershed area followed by
 723 elevation and then lake surface area. For $\delta^2\text{H}$, LASSO regression identified lake watershed
 724 area as the sole important parameter, but we also included elevation in the multiple regression
 725 as its inclusion substantially improved the regression strength. The sensitivity of $\delta^{18}\text{O}$ and
 726 $\delta^2\text{H}$ to lake watershed area probably reflects the degree of precipitation recharge the lake is
 727 receiving relative to the lake total volume (assuming that the lakes with larger surface areas
 728 generally have larger volumes). Since precipitation and the snowpack are isotopically lighter
 729 than average lake values (Figure 3a), lakes with larger watersheds will logically have greater
 730 precipitation input and thus lower $\delta^{18}\text{O}$ and $\delta^2\text{H}$ values. Lakes having lower $\delta^{18}\text{O}$ and $\delta^2\text{H}$
 731 values with higher elevation is likely a product of the altitude effect (Dansgaard, 1964;

732 Rozanski et al., 1993), and may also reflect reduced evaporation at higher elevations as
733 suggested by the δx_s results. The weak relationship observed where lakes with larger surface
734 areas are isotopically lighter is potentially because these lakes with larger surface areas tend
735 to have larger volumes, and the larger volumes of these lakes are more buffered against the
736 heavy isotope enrichment impact of evaporation. However, this weak relationship may also
737 partly arise from the positive correlation between lake surface area and watershed area ($r =$
738 0.57) since headwater lakes with smaller watersheds tend to be smaller in surface area.

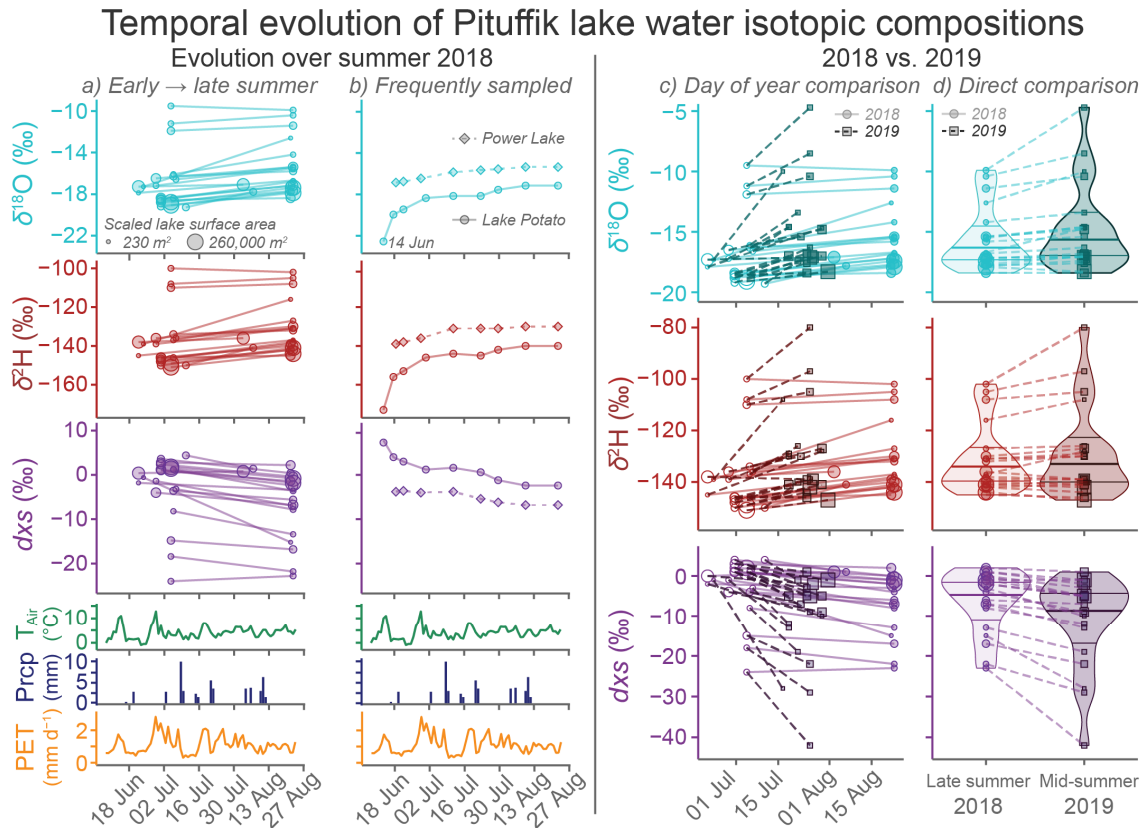
739 In contrast, δx_s is most influenced by lake surface area, followed by elevation, and finally
740 lake watershed area (Figure 7, Table S2). This strong influence of lake surface area on δx_s
741 reflects the sensitivity of small lakes to evaporation-driven isotopic effects (Kopeck et al.,
742 2018). Most of the smaller headwater and downstream lakes are shallow, and as a result,
743 these lakes' isotopic compositions can change relatively quickly under strong evaporative
744 conditions. As previously stated, these smaller lakes likely freeze to their beds in winter, and
745 these “bedfast ice” lakes melt out earlier and have longer seasonal exposure to evaporation
746 than larger lakes that have floating ice (Arp et al., 2015). Thus, the smaller lakes generally
747 greater evaporative water loss and lower δx_s values. Lakes at higher elevations have higher
748 δx_s values, suggesting that they have less evaporative impacts. This is most likely due to the
749 slightly lower temperatures at higher elevations that reduce direct evaporation and extend the
750 period of lake ice cover when no evaporation can occur. Additionally, the tundra snowpack
751 lasts longer at higher altitudes, and higher lakes will receive the high δx_s runoff from this
752 snowpack for a longer portion of the summer. Finally, lakes with larger watersheds have
753 higher δx_s values, which reflects how larger watersheds provide a greater volume of high δx_s
754 precipitation and snow melt input relative to lake volume compared to lakes in smaller
755 watersheds.

756 **5.2 Temporal variability in lake isotopes**

757 **5.2.1 Lake isotopic variability over summer 2018**

758 Over summer 2018, we observe consistent isotopic changes across the multi-annual subset of
759 18 Pituffik lakes and 2 pools (simplified hereafter to just “20 lakes”) studied for temporal
760 evolution (Figure 8a). Nearly all these lakes are isotopically heavier (19 of 20 lakes,
761 exception: Angry Duck Lake) with lower δx_s values (18 of 20 lakes, exceptions: Angry Duck
762 Lake and Lake Tuto) at the end of summer than in early summer. This change is consistent

763 with observations in other high latitude lakes where lake waters are isotopically lighter in
 764 spring and early summer due to snowpack melt inflow but become enriched in heavier
 765 isotopes by late summer due to evaporation losses (Gibson & Reid, 2014; Leng & Anderson,
 766 2003). The two lakes that did not follow this isotopic evolution can be explained by their
 767 particular lake environments: Angry Duck Lake is a very shallow endorheic lake whose
 768 isotopic composition is likely very sensitive to recent precipitation events while Lake Tuto is
 769 a large, high altitude lake less sensitive to evaporation and fed by melting snowpack well into
 770 the late summer. Although spatially, lakes with smaller surface areas are isotopically heavier
 771 with lower dxs values (Figure 7), lake surface area does not have a clear impact on the rate
 772 and magnitude of isotopic change over summer 2018 (Figure 8a).



773

774 **Figure 8.** Water isotopic composition changes in select Pituffik lakes over summers 2018 and
 775 2019. Lakes included here are part of the multi-annual subset of 18 lakes and 2 pools that
 776 were sampled during each of the three main sampling periods. The size of each point
 777 represents the relative log-scaled surface area of the lakes, which was identified as a primary
 778 factor in evaporation's impact on isotopic composition. In (a), isotopic differences in the
 779 lakes from early to late 2018 summer are shown while (b) shows the isotopic changes over

780 summer 2018 for the frequently sampled Power Lake (diamonds, dashed line) and Lake
781 Potato (circles, solid line). Daily mean air temperature, precipitation amount, and potential
782 evapotranspiration over summer 2018 are shown at the bottom of (a) and (b) for
783 environmental context (Muscarei, 2018; Singer et al., 2021; USAF, 2019). For (c) and (d),
784 interannual water isotopic differences between summer 2018 (circles) and summer 2019
785 (squares) are shown. In (c), isotopic values are plotted by sampling day of year. Lines
786 connect early summer 2018 values to late summer 2018 values (solid lines) and to mid-
787 summer 2019 (dashed lines) values for each individual lake and pool. In (d), isotopic values
788 are directly compared between late summer 2018 and mid-summer 2019 samples with overall
789 value distributions illustrated with violin plots. The isotopic values for each individual lake
790 and pool are connected by dashed lines.

791 The frequent sampling performed at Lake Potato and Power Lake grant us further insight into
792 summer lake isotopic evolution and into how short-term weather events influence isotopic
793 variability. Over summer 2018, both Lake Potato and Power Lake share increasing $\delta^{18}\text{O}$ and
794 $\delta^2\text{H}$ values and decreasing d_{xs} values (Figure 8b). Both lakes have similar LEL slopes (Lake
795 Potato: 6.1 ± 0.3 ; Power Lake: 6.0 ± 0.9), and the intersections of these LEL with the LMWL
796 estimate that the initial water isotopic compositions for Lake Potato is $\delta^{18}\text{O} = -22.9 \text{‰}$ and
797 $\delta^2\text{H} = -174 \text{‰}$ and for Power Lake is $\delta^{18}\text{O} = -23.2 \text{‰}$ and $\delta^2\text{H} = -176 \text{‰}$. These values are
798 very close to the annual amount-weighted GNIP precipitation mean values of -22.5‰ and
799 -173‰ . The excellent agreement between the three isotopic compositions (Lake Potato
800 initial water, Power Lake initial water, mean annual precipitation) gives credence to the
801 improved accuracy obtained when restricting LELs to individual water bodies rather than
802 regional aggregates and supports the close approximation of permafrost-bound tundra lakes
803 to the evaporation pan model that the technique is founded upon (Bowen et al., 2018; Gibson
804 et al., 1999).

805 Although only collected at Lake Potato, the first lake water sample taken on 14 June 2018
806 highlights the rapidly changing Pituffik hydrology during the early summer thaw. This
807 sample has the second lowest $\delta^{18}\text{O}$ and $\delta^2\text{H}$ values of any lake water sample in our database,
808 but the $\delta^{18}\text{O}$ and $\delta^2\text{H}$ values of the next sample taken only four days later increased by 2.6 ‰
809 and 17 ‰, respectively. This four-day rise is the same magnitude of isotopic change then
810 observed over the next two months in Lake Potato from 18 June to 23 August. This extreme
811 isotopic change is largely explained by the different thaw timings of the tundra snowpack and

812 the Lake Potato ice cover. On 14 June, warm and sunny conditions led to extensive snowpack
813 melt across the tundra, but Lake Potato itself maintained a nearly intact ice cover that greatly
814 limited mixing between the inflowing snow melt and the pre-existing lake water in and
815 beneath the ice. Water samples taken directly of the snowpack meltwater on this day had
816 similarly low isotopic values as the Lake Potato sample, and our sample of the near surface
817 water, therefore, simply captured mostly isotopically light snowpack melt flowing over the
818 isotopically heavier lake ice. By 18 June, the lake ice had more fully retreated, and the
819 heavier $\delta^{18}\text{O}$ and $\delta^2\text{H}$ values of this date's sample reflect the mixing in of the pre-existing
820 lake waters. In further support, the Lake Potato d_{xs} values drop from a relatively high +8 ‰
821 on 14 June (suggesting a source with limited past evaporation, such as snow melt) to +4 ‰
822 on 18 Jun (suggesting the mixing in of waters with greater past evaporation, such as lake
823 water).

824 Although the LEL slopes are similar between the Lake Potato and Power Lake, the lakes'
825 isotopic compositions evolve differently in early summer based on their upstream drainage
826 sizes and ice coverage. Lake Potato displays a strong early season thaw pulse and recovery
827 from 18 June to 01 July 2018 when the isotopically light waters supplied by snowmelt
828 become steadily heavier while d_{xs} values decrease. This thaw pulse recovery follows the
829 decreasing input of snowpack meltwater once the local snowpack disappears and the
830 continuing melt and reincorporation of the lake's isotopically heavier ice and last season's
831 deeper waters (Figure S5). In addition to the mixing in of older lake waters which carry lower
832 d_{xs} values from prior summer evaporation, new evaporation might also occur and further
833 decrease lake d_{xs} values as Lake Potato's ice cover retreated. In contrast, Power Lake has a
834 much less dramatic thaw pulse and recover, which is likely due to its much smaller drainage
835 basin (sixteen times smaller than Lake Potato) which receives snowpack meltwater only from
836 the small region directly surrounding the lake. Additionally, the d_{xs} values observed from 18
837 June to 12 July in Power Lake are very stable and likely resulted from the near-continuous ice
838 cover the lake held well into mid-July (Figure S5) which prevented any new evaporation
839 from substantially altering the lake water isotopic composition.

840 The two lakes also show different responses to precipitation events that occurred in July.
841 Nearly all ice in Lake Potato was melted by 04 July 2018 (Figure S5), and the isotopic values
842 then change very little for the rest of the month. With the lack of ice cover, we would expect
843 to observe some evaporative enrichment of heavy water isotopes under relatively high PET,

844 but the June trend of increasing $\delta^{18}\text{O}$ and $\delta^2\text{H}$ values and decreasing dxs values at Lake
845 Potato is interrupted in July by a plateauing of values less strongly observed in Power Lake
846 (Figure 8b). This plateauing may be due to a series of July rain events whose isotopic values
847 (mean $\delta^{18}\text{O}$: -19.1‰ ; $\delta^2\text{H}$: -150‰ ; dxs : $+2.6\text{‰}$) would serve to counteract any effect from
848 evaporation. With the much larger drainage basin of Lake Potato, the runoff from any
849 precipitation event would have a more magnified effect on Lake Potato water isotopes
850 compared to Power Lake.

851 Evaporative enrichment in heavier isotopes is evident in both lakes from late July through
852 mid-August. Under drier and warmer conditions with greater PET than early July, the $\delta^{18}\text{O}$
853 values of both lakes increase at the same time that dxs values decrease (Figure 8b).
854 Unusually, Power Lake's $\delta^2\text{H}$ values barely change from 12 July through the end of summer
855 despite its $\delta^{18}\text{O}$ values increasing until 10 August. This possibly reflects a situation where the
856 limited rainfall runoff that Power Lake received was isotopically balanced with regards to
857 $\delta^2\text{H}$ with evaporative loss that preferentially removes water with lighter hydrogen isotopes,
858 but we lack the ability to verify this conjecture. Finally, both lakes exhibit almost no isotopic
859 change between 10 August and the last observation on 23 August as daily mean temperatures
860 were rapidly dropping to near freezing, and evaporation was much more limited.

861 For broader applications, the isotopic observations from these two lakes can be used to
862 estimate how much temporal isotopic change might occur on short timescales, such as within
863 each of the 15–20 day long periods where we sampled our multi-annual 20 lakes subset.
864 Based on observed changes in 2018 at Lake Potato and Power Lake (Table S3), a lake
865 sampled at the beginning and end of a 20-day sampling period could see, on average, a $\delta^{18}\text{O}$
866 increase of 0.4 to 1.2 ‰, a $\delta^2\text{H}$ increase of 3.2 to 6.4 ‰, and a dxs decrease of 0.8 to 2.4 ‰.
867 Changes toward the beginning of summer might be twice these values while changes toward
868 the end of summer would more likely be near zero. We can consider these values to represent
869 a rough upper bound on the potential degree of temporal isotopic variability within a 20-day
870 sampling period, but we also note that most of our 20 lakes were sampled together with less
871 than a week's separation and thus have a limited potential impact from temporal isotopic
872 evolution.

873 **5.2.2 Interannual summer lake isotopic values in 2018 versus 2019**

874 Our 2019 lake sampling took place over the last two weeks in July, and we use the isotopic
875 composition of these samples relative to those taken in 2018 to gain insight into how lake
876 water isotopes may change from year to year. However, because the timing of the 2019
877 sampling falls between the two sampling periods in 2018, we cannot directly compare values
878 between the years because the lake isotopic composition is constantly evolving over the
879 summer. Based on observations at Potato Lake and Power Lake (Figure 8b), we assume that
880 $\delta^{18}\text{O}$ and $\delta^2\text{H}$ values in Pituffik lakes generally increase and d_{xs} values decrease from the
881 time of early season snowpack melt in late May/early June until the middle of August. Thus,
882 the isotopic values of the lakes in middle to late August should be their maximum $\delta^{18}\text{O}$ and
883 $\delta^2\text{H}$ and minimum d_{xs} values, with the degree of isotopic change over the summer primarily
884 reflecting the amount of evaporative water loss.

885 Overall, the isotopic values of our lake dataset suggest that more evaporation occurred in
886 2019 than in 2018. By late July 2019, 95% of the lakes in the multi-annual subset already had
887 lower d_{xs} values than the values measured in late August 2018, signifying greater evaporative
888 loss. Similarly, 85% and 65% of lakes had higher $\delta^{18}\text{O}$ and $\delta^2\text{H}$ values indicative of greater
889 evaporation, respectively, in late July 2019 than late August 2018 (Figure 8c–d), which is
890 expected as evaporation also enriches remaining water in heavier isotopes. For many lakes,
891 the differences in d_{xs} values between the two years were extremely large: five lakes had d_{xs}
892 values $> 7\%$ lower in 2019 than in 2018 with the largest difference of 20% lower d_{xs}
893 observed in an isolated roadside pool. Additionally, the LEL calculated from these 18 lakes
894 and 2 pools in mid-summer 2019 had a lower slope value (4.9 ± 0.2) than either early or late
895 summer 2018 (5.3 ± 0.2 and 5.1 ± 0.2 , respectively), also suggesting a more arid environment
896 existed in 2019 than in 2018 (Figure S8). All together, these values suggest that substantially
897 more evaporative water loss had occurred across Pituffik lakes by the end of July in 2019
898 than during the entire summer of 2018.

899 Weather differences between the summers 2018 and 2019 support conditions being more
900 favorable for evaporation in 2019 as we inferred from the lake isotopic compositions.
901 Weather conditions and surface melt extent in summer 2018 were close to 1981–2010
902 averages (Mote, 2020; USAF, 2019), but summer 2019 was one of the warmest and sunniest
903 seasons on record for Greenland with massive volumes of surface ice melted from the GrIS
904 across the island (Sasgen et al., 2020; Tedesco & Fettweis, 2020). Although the 2019 GrIS
905 melt peaked with an extraordinary event at the end of July, the entire summer had remarkably

906 stable anticyclonic conditions and above average surface melt (Mote, 2020; Tedesco &
907 Fettweis, 2020).

908 At Pituffik, the persistent anticyclonic conditions during June–August 2019 resulted in that
909 summer being 4.5°C warmer and having an atmospheric pressure 12 hPa higher than the
910 same period in 2018 (Muscari, 2018). Summer 2019 was also drier than summer 2018, both
911 in total precipitation (32 vs. 54 mm, respectively) and in mean relative humidity (68% vs.
912 79%, respectively) (Muscari, 2018; USAF, 2019). When totaled over each summer, modeled
913 daily PET (Singer et al., 2021) for Pituffik was almost two times greater in 2019 than 2018
914 (177 mm vs. 96 mm, respectively). Indices for the North Atlantic Oscillation and Arctic
915 Oscillation show that atmospheric circulations were very different between the two years,
916 with consistent positive indices in 2018 and consistent negative indices in 2019. A negative
917 North Atlantic Oscillation is associated with greater evaporation of Pituffik surface waters
918 due to the local foehn-like conditions as southerly winds are forced over the GrIS and Tuto
919 ice dome (Akers et al., 2020). The enhanced pressure gradients of the negative North Atlantic
920 Oscillation also drive stronger katabatic winds that also increase evaporative potential (Kopeck
921 et al., 2018). Finally, the consistently warmer conditions in 2019 brought much earlier ice-
922 free conditions to the Pituffik lakes that lengthened the evaporation exposure period, with ice
923 coverage in July 2019 running 16–20 days ahead of conditions in 2018 (Copernicus, 2019).

924 Other than evaporation, interannual lake isotopic variability has also been suggested to reflect
925 isotopic differences in the winter snowpack resulting from varying winter storm sources and
926 air temperature (Kjellman et al., 2022). Although we do not have early summer water
927 samples from 2019 to directly compare the isotopic composition of tundra snowpack
928 meltwater with our samples from 2018, we do not believe that snowpack isotopic variability
929 best explains the observed interannual differences in Pituffik lake isotopic composition. This
930 would require the 2018–2019 winter snowpack to have been isotopically heavier than the
931 2017–2018 snowpack. This seems unlikely for Pituffik because the winter 2018–2019 had a
932 colder mean air temperature and synoptic conditions which would suggest that the snowpack
933 melting in spring 2019 would more likely have lower $\delta^{18}\text{O}$ and $\delta^2\text{H}$ values than the 2018
934 spring snowpack (Akers et al., 2020). More precipitation was reported in the seven months
935 leading to June 2018 than June 2019 (53.4 vs. 29.6 mm water equivalent), possibly resulting
936 in a greater tundra snowpack water volume in 2018. Greater snowpack volume could have
937 possibly flushed the lakes with more snowmelt in 2018 than 2019 leading to isotopically

938 lighter lakes in 2018, but limits imposed by lake ice coverage and snow melt bypass (Wilcox
939 et al., 2022) likely dampen the impact of different snowpack volumes. Overall, the sheer
940 magnitude of isotopic change between 2018 and 2019, the exceptionally negative δx_s values
941 in 2019, and the lower lake LEL slope in 2019 strongly support our conclusion that the
942 isotopic differences between the 2018 and 2019 are primarily due to differences in summer
943 weather that affected evaporation rather than different snowpack isotopic compositions.

944 **6 Isotopic variability in streams**

945 The stream sites we sampled across the Pituffik region have less isotopic variability than
946 lakes (Figure 3a), but their isotopic differences can still be linked to the environmental
947 character of their watersheds. We find that the isotopic composition of a stream is most
948 clearly determined by the relative contribution of runoff from tundra snowpack melt versus
949 GrIS glacial melt, with a smaller influence also from rain events and lake water evaporation
950 in particular streams. The winter snowpack across the Pituffik tundra has distinctively low
951 $\delta^{18}\text{O}$ and $\delta^2\text{H}$ values due to its condensation at very low temperatures and a substantial rain
952 out effect during the moisture transit to northwest Greenland over sea ice and/or over the
953 GrIS (Akers et al., 2020; Dansgaard, 1964; Rozanski et al., 1993).

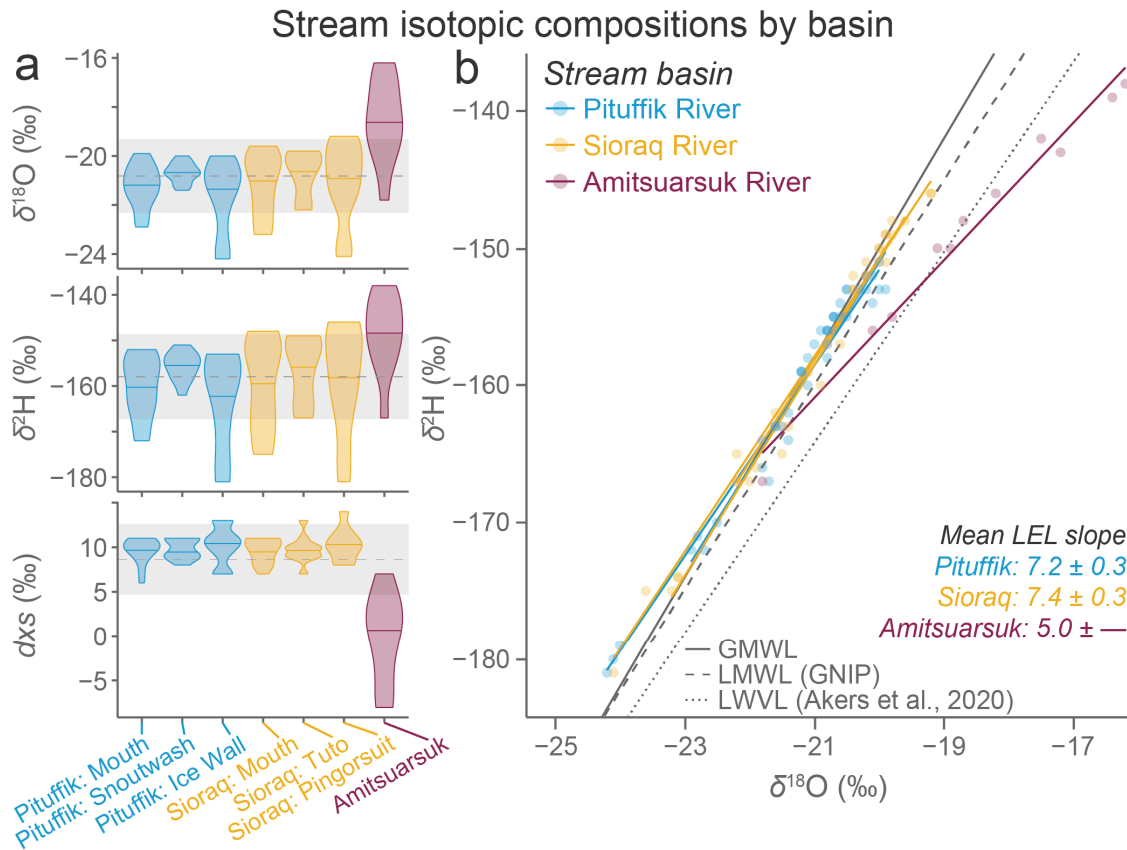
954 In contrast, $\delta^{18}\text{O}$ and $\delta^2\text{H}$ values of glacial ice from the Tuto dome and its direct meltwater
955 runoff (Akers et al., 2023a; Csank et al., 2019; Reeh et al., 1990) ($\delta^{18}\text{O} \approx -18$ to -21 ‰, $\delta^2\text{H}$
956 ≈ -138 to -156 ‰) are generally higher than the isotopic values that we observed in the
957 winter tundra snowpack ($\delta^{18}\text{O} \approx -20$ to -39 ‰, $\delta^2\text{H} \approx -138$ to -300 ‰) and in the runoff of
958 this tundra snowpack in early summer ($\delta^{18}\text{O} \approx -21$ to -23 ‰, $\delta^2\text{H} \approx -155$ to -174 ‰).
959 Although meltwater coming off the GrIS might be expected to be isotopically light due to the
960 high elevation and coldness of the ice dome, the higher GrIS isotopic values may result from
961 the fact that summer precipitation that falls as rain on the tundra will often fall as snow on the
962 GrIS. This summer snow can draw upon local moisture with relatively high $\delta^{18}\text{O}$ and $\delta^2\text{H}$
963 values from ice-free Baffin Bay (Akers et al., 2020). As a result, this seasonal difference in
964 snow origin allows us to distinguish between water sourced from tundra snowpack versus the
965 GrIS. While the snowpack on the tundra will be almost entirely biased toward low $\delta^{18}\text{O}$ and
966 $\delta^2\text{H}$ from winter snowfall, the ice of the nearby GrIS will have higher mean isotopic values
967 due to the inclusion of snow that has fallen all throughout the year, including summer.

968 In contrast to the lake studies, d_{xs} has much more limited value in stream isotopic
969 interpretation as d_{xs} values do not consistently differ between most stream water sources
970 such as the tundra snowpack and GrIS. Evaporation of source waters occurs very little for
971 streams primarily sourced by meltwater, but streams with significant lake water components
972 can be identified by their low d_{xs} values. Summer rain on the tundra has relatively high $\delta^{18}\text{O}$
973 and $\delta^2\text{H}$ values and low d_{xs} values (Figure 3a), but the small volume and intermittent
974 occurrence of rain events limit their impact in comparison to snowpack and GrIS melt for
975 most streams.

976

977 **6.1 Spatial variability in stream isotopes**

978 Generally, spatial variability in stream isotopic composition is much more limited than the
979 variability observed in lakes across Pituffik. Focusing on three stream networks that we
980 repeatedly sampled (Pituffik River, Sioraq River, Amitsuarsuk River), we note that all six
981 frequently sampled Pituffik and Sioraq River sites have broadly similar isotopic values while
982 samples from the Amitsuarsuk River have much higher $\delta^{18}\text{O}$ and $\delta^2\text{H}$ values and lower d_{xs}
983 values (Figure 9a). These isotopic values suggest that while evaporation does not
984 substantially affect the source waters supplying any site along the Pituffik or Sioraq Rivers, it
985 has clearly altered the source waters supplying the Amitsuarsuk River. The $\delta^{18}\text{O}$ vs. $\delta^2\text{H}$
986 linear regressions of the streams (i.e., their local water lines, or LWLs) (Figure 9b) support
987 this conclusion as the Pituffik and Sioraq River LWLs do not deviate from the LMWL but the
988 Amitsuarsuk River LWL forms a distinct LEL with a slope value (5.0 ± 0.5) much lower than
989 the LMWL slope (7.5 ± 0.4).



990

991 **Figure 9.** Spatial variability in the isotopic composition of Pituffik streams. Three frequent
 992 sampling sites each existed for the Pituffik and Sioraq Rivers while Amitsuarsuk River was
 993 sampled less regularly at different points along its entire stretch. Violin plots (a) show the
 994 isotopic distributions of stream water samples grouped by stream sample site. Data are
 995 plotted so that the maximum width is equivalent between groups, regardless of sample count.
 996 The mean isotopic values ± 1 standard deviation of all samples are shown by the dashed line
 997 and gray bar crossing all violins. Within each violin, the median value per site is shown by a
 998 solid horizontal line. In (b), $\delta^2\text{H}$ vs. $\delta^{18}\text{O}$ is plotted to show local evaporation lines (LELs) for
 999 each stream sampling site colored by stream basin. LEL slope value means and 95%
 1000 confidence intervals of the means are displayed for each stream basin. Note that because
 1001 Amitsuarsuk River was irregularly sampled at points along its main stem, it only has a single
 1002 LEL and no confidence interval of the mean.

1003 These differences in evaporation's isotopic impact on the streams directly result from the
 1004 spatial differences in where the streams primarily source their water. The headwaters of all
 1005 major tributaries of the Pituffik and Sioraq are sourced at the GrIS or large permanent

1006 snowfields. Unsurprisingly, the d_{xs} values at the Pituffik and Sioraq River sites are never
1007 lower than +6 ‰ and fall within values that we observed in snow and ice on the landscape
1008 (Figure 3a, Figure 9a). This d_{xs} match supports that snow and ice meltwater is consistently
1009 the primary water source for the Pituffik and Sioraq Rivers and that evaporation does not
1010 substantially impact the water supplying these streams after its original precipitation
1011 deposition. For these two streams, the volume and speed of flow from snowpack and GrIS
1012 melt apparently overwhelms any other contribution from lakes or other surface waters that
1013 would have lower d_{xs} values due to evaporative water losses or from summer precipitation.

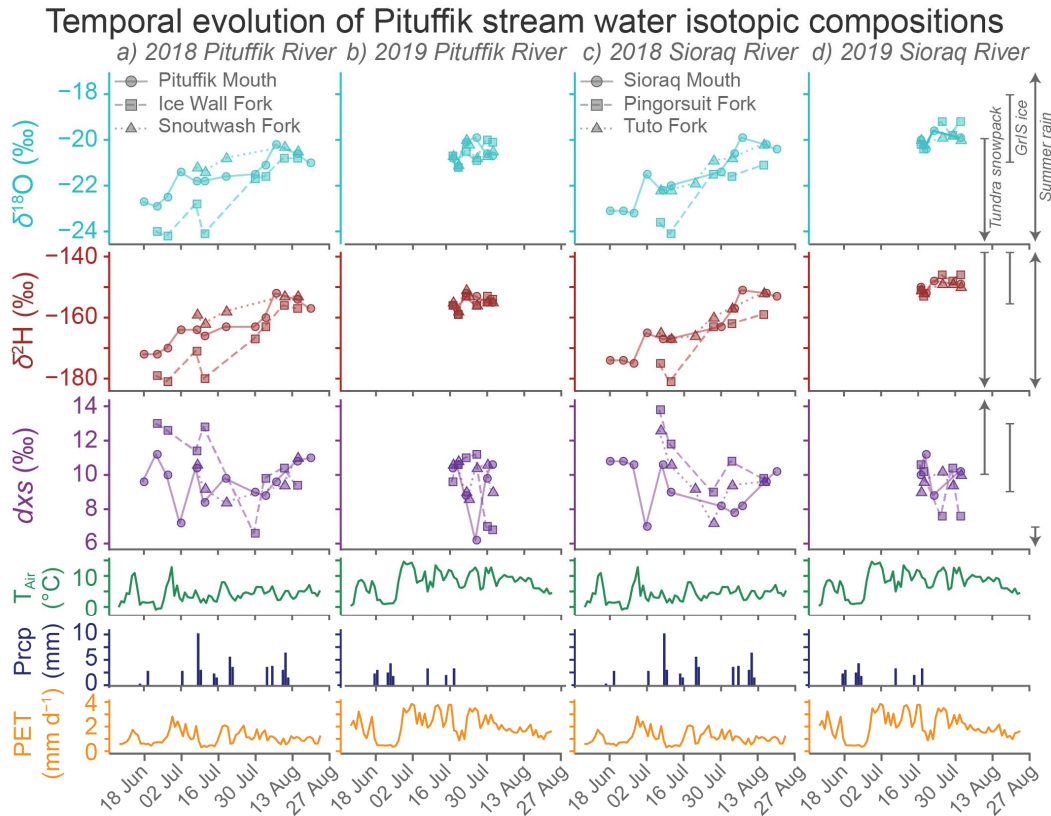
1014 In contrast, the Amitsuarsuk River has no connection to the GrIS or high elevation snow
1015 patches, but it does directly connect and drain several of the main lakes (Figure S4). The
1016 isotopically heavier $\delta^{18}\text{O}$ and $\delta^2\text{H}$ values and markedly lower d_{xs} values (−8 to +7 ‰) in the
1017 Amitsuarsuk River thus result from the stream sourcing its water primarily from lakes
1018 experiencing considerable evaporative water loss (Section 5). Indeed, the slope of the
1019 Amitsuarsuk River's LEL (5.0 ± 0.5 , Figure 9b) is within the confidence interval of the
1020 downstream lakes LEL slope (4.8 ± 0.6 , Figure 5b), confirming that the Amitsuarsuk River's
1021 water is carrying the evaporative signal created in the lakes along its course. Additionally, the
1022 d_{xs} values of the Amitsuarsuk River decrease as summer progresses (Figure S9), mimicking
1023 the evaporation-driven isotopic evolution observed in the lakes (Figure 8a–b). This is in
1024 particular contrast to the d_{xs} evolution of the Pituffik and Sioraq Rivers which lack any
1025 consistent and clear d_{xs} trend over summer (Figure S9). Finally, the four 2019 samples from
1026 the Amitsuarsuk River had lower d_{xs} values than all 2018 samples but one, and this also
1027 mimics the lake observations where waters had lower d_{xs} values in 2019 due to the greater
1028 evaporative water loss that occurred that summer (Figure 8c–d). The Pituffik and Sioraq
1029 Rivers, in contrast, show no distinct differences in d_{xs} between the two summers (Figure S9),
1030 confirming the limited impact that evaporation plays in determining the streams' isotopic
1031 compositions.

1032 **6.2 Temporal variability in stream isotopes**

1033 Our frequent sampling of the six sites along the Pituffik and Sioraq Rivers allows us to
1034 examine the isotopic evolution of these two streams over the summer thaw season. Similar to
1035 our monitoring of Lake Potato and Power Lake, the 2018 summer was almost fully captured
1036 while only two weeks were observed in 2019 (Figure 10). However, this 2019 sampling

1037 coincided with one of the largest known periods of GrIS surface melt mass loss (Cullather et
1038 al., 2020; Sasgen et al., 2020) when the Pituffik and Sioraq Rivers had extremely high
1039 discharge rates (Figure S3b, d). As discussed previously, we interpret the isotopic variability
1040 in these two streams as lower $\delta^{18}\text{O}$ and $\delta^2\text{H}$ values signifying greater tundra snowpack
1041 contribution and higher $\delta^{18}\text{O}$ and $\delta^2\text{H}$ values signifying greater GrIS contribution. The much
1042 higher variability and lack of obvious patterns in stream δx_s values makes their interpretation
1043 less certain and possibly more responsive to individual precipitation events.

1044 Similar to our lake spatial analysis, the evolution of stream isotopic compositions over time
1045 means that spatial comparison across sites is best performed with samples that were taken
1046 close together in date. For comparing water isotopes at the mouths of the Pituffik and Sioraq
1047 Rivers, we have eleven dates in 2018 and three dates in 2019 where both sites were sampled
1048 within 36 hours of each other. Overall, the mean isotopic difference between the two streams
1049 on matched days is small, with the Pituffik River having 0.2 ‰ lower $\delta^{18}\text{O}$ and 1 ‰ lower
1050 $\delta^2\text{H}$ values than the Sioraq River and no notable δx_s difference. Both these streams drain
1051 similarly large swaths of tundra and directly source meltwater from the GrIS margin, and it is
1052 therefore logical that they have similar isotopic values. The mean isotopic value of all
1053 sampled dates for these two streams ($\delta^{18}\text{O} = -21.1 \pm 0.3$ ‰, $\delta^2\text{H} = -159 \pm 2$ ‰, $\delta x_s = 10 \pm 1$ ‰)
1054 falls between values for GrIS melt and tundra snowpack, reflecting the joint contributions to
1055 streamflow from both sources.



1056

1057 **Figure 10.** Stream water isotopic value changes along the Pituffik River (a–b) and Sioraq
 1058 River (c–d) in summers 2018 and 2019. Sampling was performed at three sites on each
 1059 stream, and different site data are indicated by different icon shapes and line patterns. The
 1060 daily mean air temperature, precipitation amount, and potential evapotranspiration (Muscari,
 1061 2018; Singer et al., 2021; USAF, 2019) for the corresponding summer are provided at bottom
 1062 for environmental context. The ranges of observed isotopic values in the winter tundra
 1063 snowpack, the GrIS ice, and summer rain events are shown at far right.

1064 In the early summer, the Ice Wall Fork of the Pituffik River was isotopically lighter than the
 1065 Pituffik mouth while the Snoutwash Fork was isotopically heavier than the mouth (Figure
 1066 10a). Notably, the Ice Wall Fork predominately drains higher elevation plains and moraines
 1067 than the Snoutwash Fork, and the early season isotopic differences between the forks are
 1068 likely due to the isotopically light winter tundra snowpack lasting and contributing to
 1069 streamflow longer in the Ice Wall Fork’s watershed. A similar pattern exists for the Sioraq
 1070 River in early summer (Figure 10c) where the isotopically lighter Pingorsuit Fork drains the
 1071 highest land elevations on the peninsula (the 800+ m Pingorsuit Massif) while the
 1072 isotopically heavier Tuto Fork drains a relatively lower elevation region. By late summer, the

1073 isotopic composition of each stream's three components converged as very little residual
1074 winter tundra snowpack remains and all stream forks sourced the same regionally consistent
1075 runoff from glacial melt and precipitation.

1076 Over the 2018 summer, stream water became isotopically heavier at all Pituffik River and
1077 Sioraq River sampling sites while δx_s variability was irregular (Figure 10a, c). A similar
1078 general summer increase in $\delta^{18}\text{O}$ was also observed on the Sioraq River during summer-long
1079 sampling in 2010, 2011, and 2012 (Csank et al., 2019). Unlike the isotopic value increase
1080 observed in Lake Potato and Power Lake (Figure 8), the increase in stream isotopic values
1081 does not appear to be driven by evaporation because the Pituffik and Sioraq Rivers' δx_s
1082 values do not show a coinciding value decline. Instead, this $\delta^{18}\text{O}$ and $\delta^2\text{H}$ increase represents
1083 the shift in stream water contribution from predominantly tundra snowpack meltwater in
1084 early summer to predominantly GrIS meltwater in late summer. Over June 2018, the Pituffik
1085 and Sioraq watersheds changed from >75% snow-covered to <10% snow-covered with a
1086 major snowpack melt event on 14 June when the local air temperature reached 14°C
1087 (Copernicus, 2019; USAF, 2019) (Figure S2). Reflecting their tundra snowpack meltwater
1088 origin, the streams' isotopic values throughout June were very similar to the values of
1089 samples taken directly of snowpack runoff on 14 June, including the first Lake Potato
1090 monitoring sample (Figure 8b) taken as this runoff flooded the lake.

1091 The rate of $\delta^{18}\text{O}$ and $\delta^2\text{H}$ increase greatly slowed during July 2018 at the stream mouths
1092 (Figure 10a, c) reflecting a stable, relatively low flow system supplied by continued melting
1093 of small residual snowpack patches, limited GrIS surface melt, and precipitation events. This
1094 stable hydrology was favored by a cool and somewhat wet July 2018 with a mean air
1095 temperature of 3.9°C and measurable rain totaling 29 mm that fell on 7 days (Muscari, 2018;
1096 USAF, 2019). Some of these rain events were intense for the region, such as the two-day 13.2
1097 mm total that fell on 8–9 July, but an impact from precipitation events is difficult to clearly
1098 distinguish in the stream isotopes. Observed summer precipitation $\delta^{18}\text{O}$ and $\delta^2\text{H}$ values are
1099 generally isotopically heavier than the early summer stream values and similar to late
1100 summer stream values, and therefore some of the overall rise in stream isotopic values over
1101 the summer could also be attributed to an increased relative importance of precipitation in the
1102 stream flow.

1103 Precipitation may have a more substantial impact on stream dxs values. Our sampled summer
1104 rain events also had consistently lower dxs values than the streams (Figure 3a), and
1105 precipitation pulses may help explain some of the stream dxs variability, such as the
1106 abnormally low dxs values observed on 03 July 2018 in both the Pituffik and Sioraq River
1107 mouths. High dxs values observed in mid-July at the Ice Wall Fork of the Pituffik River and
1108 both upper forks of the Sioraq River may have resulted from late melting winter snowpack at
1109 these higher elevations or perhaps fresh snow input from a 8–9 July storm. However, most
1110 summer precipitation events at Pituffik are very small (< 5 mm), and any direct inflow from
1111 precipitation would be heavily mixed with residual snowmelt and thawing active layer water.
1112 Also, stream dxs variability cannot be entirely due to precipitation pulses because we observe
1113 a high degree of dxs variability in 2019 when no precipitation was occurring (Figure 10b, d).
1114 Overall, we would expect any isotopic impact from precipitation to be short-lived and
1115 typically overwhelmed by meltwater from either the tundra snowpack or the GrIS.

1116 Although the sampling period in 2019 was much shorter than 2018, it highlights well a
1117 sensitivity of the stream isotopic composition to the season-long weather pattern. Comparing
1118 samples taken only between 17 July and 03 August across both years, we observe that the
1119 stream sites in 2019 had consistently higher $\delta^{18}\text{O}$ and $\delta^2\text{H}$ values (mean \pm 95% confidence
1120 interval of each site's differences = $+1.1 \pm 0.4$ ‰ and $+9 \pm 3$ ‰, respectively) but no clear dxs
1121 difference ($+1 \pm 1$ ‰). We interpret this as the streams having a greater GrIS meltwater
1122 component in late July 2019 than late July 2018. Indeed, as previously stated, summer 2019
1123 was much warmer than summer 2018 with a very early loss of the tundra snowpack and
1124 limited precipitation (Figure S2). Abnormally high seasonal GrIS surface melt culminated in
1125 a near record melt event on 30–31 July 2019 (Cullather et al., 2020) when we observed GrIS
1126 meltwater drive extreme Pituffik and Sioraq River discharges that far exceeded 2018
1127 maximum flows and threatened long-established local infrastructure of bridges and roads
1128 (Figure S3). The 2019 melt event was also notable for the very low snow cover present on the
1129 local GrIS resulting in direct melt of glacial ice across vast expanses. As a result, we consider
1130 the stream water during this event to be nearly 100% GrIS sourced and to represent
1131 maximum potential meltwater-driven $\delta^{18}\text{O}$ and $\delta^2\text{H}$ values for the Pituffik and Sioraq Rivers.

1132 **7 Implications and conclusions**

1133 Our comprehensive study of the surface waters of the Pituffik region has important
1134 implications for paleoenvironmental studies that use water stable isotopes as proxies for past
1135 climate changes. Studies of this nature typically create transfer functions from modern
1136 observations of stable isotopes and environmental parameters to convert isotopic values
1137 archived in sediment or faunal remains into reconstructed climate histories (Van Hardenbroek
1138 et al., 2018). However, observational datasets are usually limited in scope by logistics and
1139 cost, particularly in the remote Arctic, and thus datasets collected over short time windows
1140 and/or limited spatial coverage are commonly assumed out of necessity to represent norms
1141 (e.g., Lasher et al., 2017, 2020; McFarlin et al., 2019). However, our study reveals that
1142 surface water isotopic values in the Pituffik region vary greatly in both time and space,
1143 particularly for lakes. As a result, a water sample taken on a single date at one body of water
1144 can neither be assumed representative for other regional water bodies nor assumed
1145 representative of the sampled body of water's isotopic composition at other dates throughout
1146 the season or even the same date in a different year.

1147 However, this does not mean that Arctic surface water isotopes are inherently too complex to
1148 perform as climate proxies. Based on our study's findings, we offer the following advice on
1149 how best to perform the modern water isotope sampling required to produce
1150 paleoenvironmental transfer functions in the Arctic. First, it is critical that water samples are
1151 taken from the source of the archived isotopes to be studied rather than assuming that
1152 samples from other water sources in the region will be similar and applicable. As lakes are
1153 the most likely source of an archived sediment record, this means that the specific lake of
1154 paleoenvironment study must be the focus of the modern sampling. Differences in lake type
1155 and hydrological connectivity can produce wildly different isotopic compositions even
1156 between lakes located <500 m apart (Figure 6a), and therefore isotope-climate relationships
1157 determined for a lake should only be applied to that specific lake alone.

1158 Secondly, sampling should ideally take place multiple times over a full thaw season in order
1159 to capture and model the seasonal evolution and environmental sensitivity of the water
1160 isotopes. In particular, lake water samples taken only on a single date risk being substantially
1161 different in isotopic composition from other dates and from the summer-long mean.
1162 However, few Arctic field campaigns can perform season-long sampling. For time-limited
1163 sampling, we recommend taking multiple samples across whatever time is available,
1164 particularly before and after major weather events to determine sensitivity to precipitation

1165 and surface flow changes. Sampling during early summer must acknowledge that snowpack
1166 melt and residual lake ice cover greatly skew lake isotopic compositions relative to their more
1167 consistent middle and late summer values.

1168 Related to this point, monitoring should ideally occur at not only the lake where the
1169 paleoclimate archive is being collected, but also more broadly across other regional lakes.
1170 This will allow researchers to establish the regional response to climate variations and
1171 determine how representative the chosen lake of focus is within the larger suite of lakes. To
1172 obtain an archived isotopic record that broadly tracks regional climate changes, the chosen
1173 lake should ideally follow the general trends of the regional set of lakes and avoid extreme
1174 sensitivities or unique isotopic and hydrological responses. However, some of these more
1175 sensitive or unique lakes may also prove ideal for a study targeting the particular climate
1176 parameter to which a lake is most responsive (e.g., targeting an endorheic or small headwater
1177 lake for evaporative water loss). Although hydrological parameters do not consistently
1178 control isotopic changes across different lake types, these lake type differences may allow us
1179 to capture different aspects of environmental change through comparative lake record study
1180 (e.g., Thomas et al., 2020). Critically, having the broader spatial context of the regional lake
1181 isotopic composition helps prevent misinterpreting or misattributing a lake's isotopic signal
1182 and enhances the insight that can be gleaned from a lake's paleoclimate archives.

1183 Thirdly, many studies assume that archived water isotopic values in Arctic lake sediments
1184 reflect the local precipitation and thus can be used to reconstruct past precipitation isotope
1185 changes. However, our findings suggest that this assumption cannot be broadly applied and
1186 must be verified for each lake. Nearly every Pituffik lake shows signs of isotopic alteration
1187 from evaporative loss, and many of the lakes that might be considered ideal for
1188 paleoenvironmental study (e.g., limited connectivity, small localized watersheds) are the most
1189 strongly impacted by evaporation. The isotopic composition of Pituffik lakes also appears to
1190 be substantially buffered against change from summer precipitation events, possibly due to
1191 the small volume of water that these events contribute relative to the existing lake volumes
1192 and the winter snowpack. As a result, the mean summer isotopic value of a lake probably best
1193 reflects a residual isotopic signal from the previous end of summer's lake water with major
1194 contributions from the prior winter's snowpack and current summer evaporation. Archived
1195 lake water isotopes might therefore be more accurately capturing temperature and moisture
1196 source changes of autumn and early winter precipitation (i.e., the predominant source of the

1197 snowpack) and/or summer temperature and humidity values that drive evaporation rather than
1198 changes in summer precipitation isotopes.

1199 Finally, while the many environmental drivers of lake isotopic variability can make it
1200 challenging to parse out which exact paleoclimate changes might have led to a given isotopic
1201 change in an individual lake, a more consistent response often emerges when comparing
1202 climate proxy variability across a suite of lakes in a region (e.g., Cluett & Thomas, 2020;
1203 Engstrom et al., 2000; Gibson & Edwards, 2002; Kopec et al., 2018; Shuman & Serravezza,
1204 2017). Given this consistency, collecting and analyzing sediment cores from multiple lakes in
1205 a given region would offer the most effective means of confidently capturing a regional
1206 climate signal. Increasing the number of cores to collect and analyze obviously brings
1207 logistical challenges, but records from multiple lakes not only reduce the uncertainty of
1208 identifying environmental drivers of isotopic change but also eliminates the risk that an
1209 observed isotopic excursion was simply a fluke incident that only affected a single lake.

1210 Our Pituffik results offer one example of the potential power of a regional lake suite
1211 approach. Pituffik lakes displayed a common isotopic response to more evaporative summer
1212 conditions in 2019 relative to 2018 (Figure 8c–d) that were favored by a shift to a strongly
1213 negative North Atlantic Oscillation phase in 2019. The consistent isotopic response across the
1214 peninsula's lakes strongly supports a connection to a regional to synoptic scale environmental
1215 driver like the North Atlantic Oscillation, but arguing the same climate connection based on
1216 an isotopic record from only a single lake would be much less certain due to the potential
1217 interference of local lake-specific influences. Looking farther afield, similarly consistent
1218 responses between lake isotopic compositions and the North Atlantic Oscillation were also
1219 reported from a study of multiple lakes in west Greenland (Kopec et al., 2018), suggesting
1220 that lake water isotopes along the western coast of Greenland might be used to produce a
1221 record of past air pressure variability over the GrIS. In this manner, placing a greater focus on
1222 examining lake isotopic records as regional sets rather than individually has much
1223 underutilized potential for Arctic paleoenvironmental and hydrological research.

1224 Overall, our study displays the high potential value of hydrological insight gained through
1225 intensive field isotopic sampling at a landscape scale. The isotopic compositions in our
1226 dataset encompass a nearly full complement of natural surface water types, and they function
1227 as a valuable base of comparison for isotopic studies in other Arctic water systems. The
1228 number, diversity, and frequency of lakes sampled in our work is, to our best knowledge,

1229 unprecedented for the High Arctic latitude of Pituffik and seldom achieved elsewhere in the
1230 Arctic and subarctic. Importantly, the numerous stream, surface flow, and snow/ice samples
1231 taken alongside the lake samples provide critical environmental context for understanding the
1232 expression and evolution of the lake water isotopes. Finally, our large comprehensive dataset
1233 can not only aid those investigating past and modern hydrologic systems, but also serve as a
1234 foundational isotopic reference point to quantify future environmental changes. We strongly
1235 believe that isotopic datasets such as ours from Pituffik will increasingly provide valuable,
1236 quantifiable markers of past conditions that can be directly compared with future isotopic
1237 samples to track rapid Arctic environmental change in a globally warming Earth.

1238

1239 **Acknowledgments**

1240 The authors declare no conflicts of interest regarding this research or publication. This project
1241 was funded by NSF Arctic Observing Network-ITEX 1504141 and Arctic Observing
1242 Network- EAGER MOSAiC 1852614 and supported in part by the inaugural UArctic
1243 Research Chairship to Jeff Welker. We greatly thank the assistance of the United States Air
1244 Force, the 821st Air Base Group at Pituffik Space Base/Thule Air Base, Vectrus, and Polar
1245 Field Services for the logistical and hosting support throughout this research. We thank
1246 Giovanni Muscari for graciously providing local Pituffik meteorological data. Special thanks
1247 go to the 821st Weather Squadron for meteorological data collection and to Hannah Bailey,
1248 Tarja Törmänen, Aino Erkinaro, and Kaisa-Riikka Mustonen for assisting with isotope
1249 analysis. We also thank Niels Jákup Korsgaard for his help in finding and accessing archived
1250 aerial photographs for Pituffik.

1251

1252 **Availability statement**

1253 All data and code used in this article's analyses and figure creation, including the full water
1254 isotopic dataset, are openly available online in an Zenodo repository via
1255 <https://doi.org/10.5281/zenodo.8262359> (Akers et al., 2023a) and also through PANGAEA
1256 (*repository submission currently in progress*). Geospatial data created for the Pituffik region
1257 and used in this article's analyses and figures are also openly available either as part of a new

1258 geospatial database available on GitHub via <https://doi.org/10.5281/zenodo.8256756> (Akers
1259 et al., 2023b) or through existing resources also available online (Copernicus, 2019; Howat,
1260 2019; Korsgaard et al., 2016; Porter et al., 2019).

1261

1262 **References**

- 1263 Akers, P. D., Kopec, B. G., Mattingly, K. S., Klein, E. S., Causey, D., & Welker, J. M.
1264 (2020). Baffin Bay sea ice extent and synoptic moisture transport drive water vapor
1265 isotope ($\delta^{18}\text{O}$, $\delta^2\text{H}$, and deuterium excess) variability in coastal northwest Greenland.
1266 *Atmospheric Chemistry and Physics*, 20(22), 13929–13955.
1267 <https://doi.org/10.5194/acp-20-13929-2020>
- 1268 Akers, P. D., Kopec, B. G., Klein, E. S., & Welker, J. M. (2023a). Pituffik 2018–2019 surface
1269 water stable isotope data and analyses (v1.1) (Version v1.1) [Data set]. Zenodo.
1270 <https://doi.org/10.5281/zenodo.8262359>
- 1271 Akers, P. D., Kopec, B. G., Klein, E. S., & Welker, J. M. (2023b). Pituffik, Greenland,
1272 hydrological geopackage (v1.0.1) (Version v1.0.1) [Data set]. Zenodo.
1273 <https://doi.org/10.5281/zenodo.8256756>
- 1274 Amstrup, N. (1997). Grønland under den kolde krig. Dansk og amerikansk sikkerhedspolitik
1275 1945-1968, 1-2, 1-2, København: Dansk Udenrigspolitisk Institut, 1997, 614+473 s.,
1276 kr. 395,00. *Politica*, 29(2), 215. <https://doi.org/10.7146/politica.v29i2.68132>
- 1277 Anderson, L., Birks, J., Rover, J., & Guldager, N. (2013). Controls on recent Alaskan lake
1278 changes identified from water isotopes and remote sensing. *Geophysical Research*
1279 *Letters*, 40(13), 3413–3418. <https://doi.org/10.1002/grl.50672>
- 1280 Anderson, N. J., Saros, J. E., Bullard, J. E., Cahoon, S. M. P., McGowan, S., Bagshaw, E. A.,
1281 et al. (2017). The Arctic in the Twenty-First Century: changing biogeochemical
1282 linkages across a paraglacial landscape of Greenland. *BioScience*, 67(2), 118–133.
1283 <https://doi.org/10.1093/biosci/biw158>
- 1284 Arp, C. D., Jones, B. M., Liljedahl, A. K., Hinkel, K. M., & Welker, J. M. (2015). Depth, ice
1285 thickness, and ice-out timing cause divergent hydrologic responses among Arctic
1286 lakes. *Water Resources Research*, 51(12), 9379–9401.
1287 <https://doi.org/10.1002/2015WR017362>
- 1288 Bailey, H., Hubbard, A., Klein, E. S., Mustonen, K.-R., Akers, P. D., Marttila, H., & Welker,
1289 J. M. (2021). Arctic sea-ice loss fuels extreme European snowfall. *Nature Geoscience*,
1290 14(5), 283–288. <https://doi.org/10.1038/s41561-021-00719-y>

- 1291 Bhatt, U. S., Walker, D. A., Raynolds, M. K., Bieniek, P. A., Epstein, H. E., Comiso, J. C., et al. (2017). Changing seasonality of panarctic tundra vegetation in relationship to
1292 climatic variables. *Environmental Research Letters*, *12*(5), 055003.
1293
- 1294 Bintanja, R., & Selten, F. M. (2014). Future increases in Arctic precipitation linked to local
1295 evaporation and sea-ice retreat. *Nature*, *509*(7501), 479-+.
1296 <https://doi.org/10.1038/nature13259>
- 1297 Bonne, J.-L., Masson-Delmotte, V., Cattani, O., Delmotte, M., Risi, C., Sodemann, H., &
1298 Steen-Larsen, H. C. (2014). The isotopic composition of water vapour and
1299 precipitation in Ivittuut, southern Greenland. *Atmospheric Chemistry and Physics*,
1300 *14*(9), 4419–4439. <https://doi.org/10.5194/acp-14-4419-2014>
- 1301 Bowen, G. J., Putman, A., Brooks, J. R., Bowling, D. R., Oerter, E. J., & Good, S. P. (2018).
1302 Inferring the source of evaporated waters using stable H and O isotopes. *Oecologia*,
1303 *187*(4), 1025–1039. <https://doi.org/10.1007/s00442-018-4192-5>
- 1304 Box, J. E., Colgan, W. T., Christensen, T. R., Schmidt, N. M., Lund, M., Parmentier, F.-J.
1305 W., et al. (2019). Key indicators of Arctic climate change: 1971–2017. *Environmental*
1306 *Research Letters*, *14*(4), 045010. <https://doi.org/10.1088/1748-9326/aafc1b>
- 1307 Buchwal, A., Sullivan, P. F., Macias-Fauria, M., Post, E., Myers-Smith, I. H., Stroeve, J. C.,
1308 et al. (2020). Divergence of Arctic shrub growth associated with sea ice decline.
1309 *Proceedings of the National Academy of Sciences*, *117*(52), 33334–33344.
1310 <https://doi.org/10.1073/pnas.2013311117>
- 1311 Burnham, K. K., Sinnott, D. R., Johnson, J. A., Burnham, J. L., Baroch, J. A., & Konkell, B.
1312 W. (2014). New species records and changes in abundance of waterfowl in northwest
1313 Greenland. *Polar Biology*, *37*(9), 1289–1300. [https://doi.org/10.1007/s00300-014-](https://doi.org/10.1007/s00300-014-1520-z)
1314 [1520-z](https://doi.org/10.1007/s00300-014-1520-z)
- 1315 Casado, M., Landais, A., Masson-Delmotte, V., Genthon, C., Kerstel, E., Kassi, S., et al.
1316 (2016). Continuous measurements of isotopic composition of water vapour on the
1317 EastAntarctic Plateau. *Atmospheric Chemistry and Physics*, *16*(13), 8521–8538.
1318 <https://doi.org/10.5194/acp-16-8521-2016>
- 1319 Clark, E. F. (1965). *Camp Century: Evolution of concept and history of design, construction,*
1320 *and performance* (Technical Report No. 174). Hanover, New Hampshire, USA: U.S.
1321 Army Material Command, Cold Regions Research and Engineering Laboratory.
- 1322 Clark, I. D., & Fritz, P. (1997). *Environmental Isotopes in Hydrogeology* (1st ed.). Boca
1323 Raton: CRC Press. Retrieved from <https://doi.org/10.1201/9781482242911>
- 1324 Cluett, A. A., & Thomas, E. K. (2020). Resolving combined influences of inflow and
1325 evaporation on western Greenland lake water isotopes to inform paleoclimate

- 1326 inferences. *Journal of Paleolimnology*, 63(4), 251–268.
1327 <https://doi.org/10.1007/s10933-020-00114-4>
- 1328 Colgan, W., Machguth, H., MacFerrin, M., Colgan, J. D., van As, D., & MacGregor, J. A.
1329 (2016). The abandoned ice sheet base at Camp Century, Greenland, in a warming
1330 climate. *Geophysical Research Letters*, 43(15), 8091–8096.
1331 <https://doi.org/10.1002/2016GL069688>
- 1332 Copernicus. (2019). Sentinel-2 data, Sentinel Hub. Retrieved August 15, 2019, from
1333 <https://www.sentinel-hub.com/>
- 1334 Corbett, L. B., Bierman, P. R., Lasher, G. E., & Rood, D. H. (2015). Landscape chronology
1335 and glacial history in Thule, northwest Greenland. *Quaternary Science Reviews*, 109,
1336 57–67. <https://doi.org/10.1016/j.quascirev.2014.11.019>
- 1337 Craig, H. (1961). Isotopic variations in meteoric waters. *Science*, 133(3465), 1702.
- 1338 Craig, H., & Gordon, L. I. (1965). Deuterium and oxygen 18 variations in the ocean and the
1339 marine atmosphere. In E. Tongiorgi (Ed.), *Stable Isotopes in Oceanographic Studies
1340 and Paleotemperatures* (pp. 9–130). Spoleto, Italy: Consiglio nazionale delle ricerche,
1341 Laboratorio di geologica nucleare.
- 1342 Csank, A. Z., Czimczik, C. I., Xu, X., & Welker, J. M. (2019). Seasonal patterns of riverine
1343 carbon sources and export in NW Greenland. *Journal of Geophysical Research:
1344 Biogeosciences*, 124(4), 840–856. <https://doi.org/10.1029/2018JG004895>
- 1345 Cullather, R. I., Andrews, L. C., Croteau, M. J., Digirolamo, N. E., Hall, D. K., Lim, Y., et al.
1346 (2020). Anomalous circulation in July 2019 resulting in mass loss on the Greenland
1347 ice sheet. *Geophysical Research Letters*, 47(17), e2020GL08726.
1348 <https://doi.org/10.1029/2020GL087263>
- 1349 Cuyler, C., Virk, K. S., Clausen, T. B., Jensen, F. H., Born, E. W., Laidre, K. L., & Wiig, Ø.
1350 (2022). *2017 status muskoxen (Ovibos moschatus) Cape Atholl, Thule region
1351 Greenland* (Technical Report No. 104) (p. 60). Pinngortitaleriffik – Greenland
1352 Institute of Natural Resources. Retrieved from 87-91214-81-5
- 1353 Daniels, W. C., Russell, J. M., Morrill, C., Longo, W. M., Giblin, A. E., Holland-Stergar, P.,
1354 et al. (2021). Lacustrine leaf wax hydrogen isotopes indicate strong regional climate
1355 feedbacks in Beringia since the last ice age. *Quaternary Science Reviews*, 269,
1356 107130. <https://doi.org/10.1016/j.quascirev.2021.107130>
- 1357 Dansgaard, W. (1964). Stable isotopes in precipitation. *Tellus*, 16(4), 436–468.
1358 <https://doi.org/10.1111/j.2153-3490.1964.tb00181.x>

- 1359 Dansgaard, W., Johnsen, S. J., Møller, J., & Langway, C. C. (1969). One thousand centuries
1360 of climatic record from Camp Century on the Greenland Ice Sheet. *Science*,
1361 *166*(3903), 377.
- 1362 Davies, W. E., & Reitzel, C. A. (1963). *Geology of the North Star Bugt Area, Northwest*
1363 *Greenland*. C.A. Reitzels Forlag. Retrieved from
1364 <https://books.google.ie/books?id=OCA7xgEACAAJ>
- 1365 Davis, R. M. (1966). *Design, construction and performance data of utility systems, Thule Air*
1366 *Base* (Special Report No. 95) (pp. 1–62). Hanover, New Hampshire, USA: U.S. Army
1367 Material Command, Cold Regions Research and Engineering Laboratory.
- 1368 Engstrom, D. R., Fritz, S. C., Almendinger, J. E., & Juggins, S. (2000). Chemical and
1369 biological trends during lake evolution in recently deglaciated terrain. *Nature*,
1370 *408*(6809), 161–166. <https://doi.org/10.1038/35041500>
- 1371 Eriksson, M., Holm, E., Roos, P., & Dahlgaard, H. (2004). Distribution and flux of Pu-238,
1372 Pu-239, Pu-240, Am-241, Cs-137 and Pb-210 to high arctic lakes in the Thule district
1373 (Greenland). *Journal of Environmental Radioactivity*, *75*(3), 285–299.
1374 <https://doi.org/10.1016/j.jenvrad.2003.12.007>
- 1375 Farquharson, L. M., Romanovsky, V. E., Cable, W. L., Walker, D. A., Kokelj, S. V., &
1376 Nicolsky, D. (2019). Climate change drives widespread and rapid thermokarst
1377 development in very cold permafrost in the Canadian High Arctic. *Geophysical*
1378 *Research Letters*, *46*(12), 6681–6689. <https://doi.org/10.1029/2019GL082187>
- 1379 Funder, S. (1990). Late Quaternary stratigraphy and glaciology in the Thule area, Northwest
1380 Greenland (p. 64). Museum Tusulanum Press.
- 1381 Gat, J. R. (1996). Oxygen and hydrogen isotopes in the hydrologic cycle. *Annual Review of*
1382 *Earth and Planetary Sciences*, *24*(1), 225–262.
- 1383 Gibson, J. J. (2002). Short-term evaporation and water budget comparisons in shallow Arctic
1384 lakes using non-steady isotope mass balance. *Journal of Hydrology*, *264*(1), 242–261.
1385 [https://doi.org/10.1016/S0022-1694\(02\)00091-4](https://doi.org/10.1016/S0022-1694(02)00091-4)
- 1386 Gibson, J. J., & Edwards, T. W. D. (2002). Regional water balance trends and evaporation-
1387 transpiration partitioning from a stable isotope survey of lakes in northern Canada.
1388 *Global Biogeochemical Cycles*, *16*(2). <https://doi.org/10.1029/2001GB001839>
- 1389 Gibson, J. J., & Reid, R. (2014). Water balance along a chain of tundra lakes: A 20-year
1390 isotopic perspective. *Journal of Hydrology*, *519*, 2148–2164.
1391 <https://doi.org/10.1016/j.jhydrol.2014.10.011>

- 1392 Gibson, J. J., Reid, R., & Spence, C. (1998). A six-year isotopic record of lake evaporation at
1393 a mine site in the Canadian subarctic: results and validation. *Hydrological Processes*,
1394 *12*(10–11), 1779–1792. [https://doi.org/10.1002/\(SICI\)1099-](https://doi.org/10.1002/(SICI)1099-1085(199808/09)12:10/11<1779::AID-HYP694>3.0.CO;2-7)
1395 [1085\(199808/09\)12:10/11<1779::AID-HYP694>3.0.CO;2-7](https://doi.org/10.1002/(SICI)1099-1085(199808/09)12:10/11<1779::AID-HYP694>3.0.CO;2-7)
- 1396 Gibson, J. J., Edwards, T. W. D., & Prowse, T. D. (1999). Pan-derived isotopic composition
1397 of atmospheric water vapour and its variability in northern Canada. *Journal of*
1398 *Hydrology*, *217*(1–2), 55–74. [https://doi.org/10.1016/S0022-1694\(99\)00015-3](https://doi.org/10.1016/S0022-1694(99)00015-3)
- 1399 Gibson, J. J., Birks, S. J., & Yi, Y. (2016). Stable isotope mass balance of lakes: a
1400 contemporary perspective. *Quaternary Science Reviews*, *131*, 316–328.
1401 <https://doi.org/10.1016/j.quascirev.2015.04.013>
- 1402 Gimeno, L., Vázquez, M., Eiras-Barca, J., Sorí, R., Algarra, I., & Nieto, R. (2019).
1403 Atmospheric moisture transport and the decline in Arctic Sea ice. *WIREs Climate*
1404 *Change*, *10*(4). <https://doi.org/10.1002/wcc.588>
- 1405 Gonfiantini, R. (1986). Environmental isotopes in lake studies. In P. Fritz & J. C. Fontes
1406 (Eds.), *Handbook of environmental isotope geochemistry: the terrestrial environment*
1407 (pp. 113–168). New York: Elsevier.
- 1408 Gronnow, B. (2016). Living at a High Arctic polynya: Inughuit settlement and subsistence
1409 around the North Water during the Thule Station Period, 1910–53. *Arctic*, *69*(1).
1410 <https://doi.org/10.14430/arctic4573>
- 1411 Hansen, B. L., & Langway, C. C. (1966). Deep core drilling in ice and core analysis at Camp
1412 Century, Greenland, 1961–66. *Antarctic Journal of the United States*, *1*(5), 207–208.
- 1413 Hastrup, K., Andersen, A. O., Grønnow, B., & Heide-Jørgensen, M. P. (2018). Life around
1414 the North Water ecosystem: Natural and social drivers of change over a millennium.
1415 *Ambio*, *47*(2), 213–225. <https://doi.org/10.1007/s13280-018-1028-9>
- 1416 Hauser, D. D. W., Whiting, A. V., Mahoney, A. R., Goodwin, J., Harris, C., Schaeffer, R. J.,
1417 et al. (2021). Co-production of knowledge reveals loss of Indigenous hunting
1418 opportunities in the face of accelerating Arctic climate change. *Environmental*
1419 *Research Letters*, *16*(9), 095003. <https://doi.org/10.1088/1748-9326/ac1a36>
- 1420 Heide-Jørgensen, M. P., Sinding, M. H. S., Nielsen, N. H., Rosing-Asvid, A., & Hansen, R.
1421 G. (2016). Large numbers of marine mammals winter in the North Water polynya.
1422 *Polar Biology*, *39*(9), 1605–1614.
- 1423 Hiltunen, T. A., Stien, A., Väisänen, M., Ropstad, E., Aspi, J. O., & Welker, J. M. (2022).
1424 Svalbard reindeer winter diets: Long-term dietary shifts to graminoids in response to a
1425 changing climate. *Global Change Biology*, *28*(23), 7009–7022.
1426 <https://doi.org/10.1111/gcb.16420>

- 1427 Historiske Kort. (2023). Historiske Kort: Flyfotos [Data set]. Styrelsen for Dataforsyning og
1428 Infrastruktur. Retrieved from <https://historiskekort.dk/>
- 1429 Howat, I. M. (2019). MEaSURES Greenland Ice Mapping Project (GIMP) Land Ice and
1430 Ocean Classification Mask, Version 1, 90 m x 90 m. *NASA NSIDC Distributed Active*
1431 *Archive Center*. <https://doi.org/10.5067/B8X58MQBFUPA>
- 1432 Howat, I. M., Negrete, A., & Smith, B. E. (2014). The Greenland Ice Mapping Project
1433 (GIMP) land classification and surface elevation data sets. *The Cryosphere*, 8(4),
1434 1509–1518.
- 1435 IAEA/WMO. (2022). Global Network of Isotopes in Precipitation. The GNIP Database.
1436 Accessible at: <https://nucleus.iaea.org/wiser>.
- 1437 Jenness, D. (1925). A new Eskimo culture in Hudson Bay. *Geographical Review*, 15(3), 428–
1438 437. <https://doi.org/10.2307/208564>
- 1439 Jespersen, R. G., Leffler, A. J., Oberbauer, S. F., & Welker, J. M. (2018). Arctic plant
1440 ecophysiology and water source utilization in response to altered snow: isotopic
1441 ($\delta^{18}\text{O}$ and $\delta^2\text{H}$) evidence for meltwater subsidies to deciduous shrubs. *Oecologia*,
1442 187(4), 1009–1023. <https://doi.org/10.1007/s00442-018-4196-1>
- 1443 Jespersen, R. G., Leffler, A. J., Väisänen, M., & Welker, J. M. (2022). Resistance and change
1444 in a High Arctic ecosystem, NW Greenland: Differential sensitivity of ecosystem
1445 metrics to 15 years of experimental warming and wetting. *Global Change Biology*,
1446 28(5), 1853–1869. <https://doi.org/10.1111/gcb.16027>
- 1447 Jonsson, C. E., Leng, M. J., Rosqvist, G. C., Seibert, J., & Arrowsmith, C. (2009). Stable
1448 oxygen and hydrogen isotopes in sub-Arctic lake waters from northern Sweden.
1449 *Journal of Hydrology*, 376(1–2), 143–151.
1450 <https://doi.org/10.1016/j.jhydrol.2009.07.021>
- 1451 Kendall, C., & McDonnell, J. J. (1998). *Isotope Tracers in Catchment Hydrology* (1st ed.).
1452 Amsterdam, Netherlands: Elsevier. Retrieved from [https://doi.org/10.1016/C2009-0-](https://doi.org/10.1016/C2009-0-10239-8)
1453 [10239-8](https://doi.org/10.1016/C2009-0-10239-8)
- 1454 Kjellman, S. E., Thomas, E. K., & Schomacker, A. (2022). Arctic and sub-Arctic lake water
1455 $\delta^2\text{H}$ and $\delta^{18}\text{O}$ along a coastal-inland transect: Implications for interpreting water
1456 isotope proxy records. *Journal of Hydrology*, 607, 127556.
1457 <https://doi.org/10.1016/j.jhydrol.2022.127556>
- 1458 Kopec, B. G., Feng, X., Posmentier, E. S., Chipman, J. W., & Virginia, R. A. (2018). Use of
1459 principal component analysis to extract environmental information from lake water
1460 isotopic compositions. *Limnology and Oceanography*, 63(3), 1340–1354.
1461 <https://doi.org/10.1002/lno.10776>

- 1462 Kopec, B. G., Lauder, A. M., Posmentier, E. S., & Feng, X. (2019). The diel cycle of water
1463 vapor in west Greenland. *Journal of Geophysical Research: Atmospheres*, *119*(15),
1464 9386–9399.
- 1465 Korsgaard, N. J., Nuth, C., Khan, S. A., Kjeldsen, K. K., Bjørk, A. A., Schomacker, A., &
1466 Kjær, K. H. (2016). Digital elevation model and orthophotographs of Greenland based
1467 on aerial photographs from 1978–1987. *Scientific Data*, *3*(1), 160032.
1468 <https://doi.org/10.1038/sdata.2016.32>
- 1469 Lasher, G. E., Axford, Y., McFarlin, J. M., Kelly, M. A., Osterberg, E. C., & Berkelhammer,
1470 M. B. (2017). Holocene temperatures and isotopes of precipitation in northwest
1471 Greenland recorded in lacustrine organic materials. *Quaternary Science Reviews*, *170*,
1472 45–55. <https://doi.org/10.1016/j.quascirev.2017.06.016>
- 1473 Lasher, G. E., Axford, Y., Masterson, A. L., Berman, K., & Larocca, L. J. (2020). Holocene
1474 temperature and landscape history of southwest Greenland inferred from isotope and
1475 geochemical lake sediment proxies. *Quaternary Science Reviews*, *239*, 106358.
1476 <https://doi.org/10.1016/j.quascirev.2020.106358>
- 1477 Leffler, A. J., & Welker, J. M. (2013). Long-term increases in snow pack elevate leaf N and
1478 photosynthesis in *Salix arctica*: Responses to a snow fence experiment in the High
1479 Arctic of NW Greenland. *Environmental Research Letters*, *8*(2), 025023.
- 1480 Leng, M. J., & Anderson, N. J. (2003). Isotopic variation in modern lake waters from western
1481 Greenland. *The Holocene*, *13*(4), 605–611.
1482 <https://doi.org/10.1191/0959683603hl620rr>
- 1483 Linderholm, H. W., Nicolle, M., Francus, P., Gajewski, K., Helama, S., Korhola, A., et al.
1484 (2018). Arctic hydroclimate variability during the last 2000 years: Current
1485 understanding and research challenges. *Climate of the Past*, *14*(4), 473–514.
1486 <https://doi.org/10.5194/cp-14-473-2018>
- 1487 Lupascu, M., Welker, J. M., Seibt, U., Maseyk, K., Xu, X., & Czimczik, C. I. (2014). High
1488 Arctic wetting reduces permafrost carbon feedbacks to climate warming. *Nature*
1489 *Climate Change*, *4*(1), 51–55. <https://doi.org/10.1038/NCLIMATE2058>
- 1490 MacDonald, L. A., Wolfe, B. B., Turner, K. W., Anderson, L., Arp, C. D., Birks, S. J., et al.
1491 (2017). A synthesis of thermokarst lake water balance in high-latitude regions of
1492 North America from isotope tracers. *Arctic Science*, *3*(2), 118–149.
1493 <https://doi.org/10.1139/as-2016-0019>
- 1494 MacGregor, J. A., Fahnestock, M. A., Colgan, W. T., Larsen, N. K., Kjeldsen, K. K., &
1495 Welker, J. M. (2020). The age of surface-exposed ice along the northern margin of the
1496 Greenland Ice Sheet. *Journal of Glaciology*, *66*(258), 667–684.
1497 <https://doi.org/10.1017/jog.2020.62>

- 1498 McFarlin, J. M., Axford, Y., Masterson, A. L., & Osburn, M. R. (2019). Calibration of
1499 modern sedimentary $\delta^2\text{H}$ plant wax-water relationships in Greenland lakes.
1500 *Quaternary Science Reviews*, 225, 105978.
1501 <https://doi.org/10.1016/j.quascirev.2019.105978>
- 1502 Mellat, M., Bailey, H., Mustonen, K.-R., Marttila, H., Klein, E. S., Gribanov, K., et al.
1503 (2021). Hydroclimatic controls on the isotopic ($\delta^{18}\text{O}$, $\delta^2\text{H}$, d-excess) traits of pan-
1504 Arctic summer rainfall events. *Frontiers in Earth Science*, 9, 651731.
1505 <https://doi.org/10.3389/feart.2021.651731>
- 1506 Merlivat, L., & Jouzel, J. (1979). Global climatic interpretation of the deuterium-oxygen 18
1507 relationship for precipitation. *Journal of Geophysical Research: Oceans*, 84(C8),
1508 5029–5033. <https://doi.org/10.1029/JC084iC08p05029>
- 1509 Mosbech, A., Johansen, K. L., Davidson, T. A., Appelt, M., Grønnow, B., Cuyler, C., et al.
1510 (2018). On the crucial importance of a small bird: The ecosystem services of the little
1511 auk (Alle alle) population in Northwest Greenland in a long-term perspective. *Ambio*,
1512 47(2), 226–243. <https://doi.org/10.1007/s13280-018-1035-x>
- 1513 Mote, T. L. (2020, February 26). MEaSUREs Greenland Surface Melt Daily 25 km EASE-
1514 Grid 2.0, version 1. NASA National Snow and Ice Data Center. Retrieved from
1515 <https://doi.org/10.5067/MEASURES/CRYOSPHERE/nsidc-0533.001>
- 1516 Muhic, F., Ala-Aho, P., Noor, K., Welker, J. M., Klöve, B., & Marttila, H. (2023). Flushing
1517 or mixing? Stable water isotopes reveal differences in Arctic forest and peatland soil
1518 water seasonality. *Hydrological Processes*, 37(1), e14811.
1519 <https://doi.org/10.1002/hyp.14811>
- 1520 Müller, L., Horwath, M., Scheinert, M., Mayer, C., Ebermann, B., Floricioiu, D., et al.
1521 (2021). Surges of Harald Moltke Bræ, north-western Greenland: seasonal modulation
1522 and initiation at the terminus. *The Cryosphere*, 15(7), 3355–3375.
1523 <https://doi.org/10.5194/tc-15-3355-2021>
- 1524 Muscari, G. (2018). Ground meteorological data (T, P, RH) obtained during the YOPP SOP
1525 in early 2018 at Thule Air Base, Greenland. *Istituto Nazionale Di Geofisica e*
1526 *Vulcanologia, Roma, Italy, PANGAEA*, <https://doi.org/10.1594/PANGAEA.895059>.
- 1527 Nghiem, S. V., Hall, D. K., Mote, T. L., Tedesco, M., Albert, M. R., Keegan, K., et al.
1528 (2012). The extreme melt across the Greenland ice sheet in 2012. *Geophysical*
1529 *Research Letters*, 39(20). <https://doi.org/10.1029/2012gl053611>
- 1530 Nichols, R. L. (1953). Geomorphic observations at Thule, Greenland, and Resolute Bay,
1531 Cornwallis Island, NWT. *American Journal of Science*, 251(4).
1532 <https://doi.org/10.2475/ajs.251.4.268>

- 1533 Noor, K., Marttila, H., Klöve, B., Welker, J. M., & Ala-aho, P. (2023). The spatiotemporal
1534 variability of snowpack and snowmelt water ¹⁸O and ²H isotopes in a subarctic
1535 catchment. *Water Resources Research*, 59(1), e2022WR033101.
1536 <https://doi.org/10.1029/2022WR033101>
- 1537 Oqaasileriffik. (2022). Oqaasileriffik: The Language Secretariat of Greenland. Retrieved May
1538 1, 2022, from <https://oqaasileriffik.gl/>
- 1539 Petersen, N. (2008). The Iceman that never came. *Scandinavian Journal of History*, 33(1),
1540 75–98. <https://doi.org/10.1080/03468750701449554>
- 1541 PGC. (2019, August 15). ArcticDEM-Polar Geospatial Center. Retrieved August 15, 2019,
1542 from <https://www.pgc.umn.edu/data/arcticdem/>
- 1543 Porter, C., Morin, P., Howat, I., Noh, M. J., Bates, B., Peterman, K., et al. (2019).
1544 ArcticDEM, V3.0, Release 7. <https://doi.org/10.7910/DVN/OHHUKH>
- 1545 Putman, A. L., Fiorella, R. P., Bowen, G. J., & Cai, Z. (2019). A global perspective on local
1546 meteoric water lines: Meta-analytic insight into fundamental controls and practical
1547 constraints. *Water Resources Research*, 55(8), 6896–6910.
1548 <https://doi.org/10.1029/2019WR025181>
- 1549 Reeh, N., Thomsen, H. H., Frich, P., & Clausen, H. B. (1990). Stable isotope studies on ice
1550 margins in the Thule area. In S. Funder (Ed.), *Late Quaternary stratigraphy and*
1551 *glaciology in the Thule area, Northwest Greenland* (Vol. 22, pp. 47–56). Meddelelser
1552 Om Grønland, Geosicence.
- 1553 Ries, C. J. (2012). On frozen ground: William E. Davies and the military geology of northern
1554 Greenland 1952–1960. *The Polar Journal*, 2(2), 334–357.
1555 <https://doi.org/10.1080/2154896X.2012.735044>
- 1556 Rozanski, K., Araguás-Araguás, L., & Gonfiantini, R. (1993). Isotopic patterns in modern
1557 global precipitation. In *Climate Change in Continental Isotopic Records* (pp. 1–36).
1558 Retrieved from <https://doi.org/10.1029/GM078p0001>
- 1559 Sasgen, I., Wouters, B., Gardner, A. S., King, M. D., Tedesco, M., Landerer, F. W., et al.
1560 (2020). Return to rapid ice loss in Greenland and record loss in 2019 detected by the
1561 GRACE-FO satellites. *Communications Earth & Environment*, 1(1), 8.
1562 <https://doi.org/10.1038/s43247-020-0010-1>
- 1563 Sauer, P. E., Miller, G. H., & Overpeck, J. T. (2001). Oxygen isotope ratios of organic matter
1564 in arctic lakes as a paleoclimate proxy: field and laboratory investigations. *Journal of*
1565 *Paleolimnology*, 25(1), 43–64. <https://doi.org/10.1023/A:1008133523139>

- 1566 Schytt, V. (1955). *Glaciological investigations in the Thule Ramp area* (Sipre Report No. 28)
1567 (p. 88). Wilmette, Illinois, USA: Snow, Ice and Permafrost Research Establishment,
1568 Corps of Engineers, U.S. Army.
- 1569 Serreze, M. C., & Barry, R. G. (2011). Processes and impacts of Arctic amplification: A
1570 research synthesis. *Global and Planetary Change*, 77(1–2), 85–96.
1571 <https://doi.org/10.1016/j.gloplacha.2011.03.004>
- 1572 Shuman, B. N., & Serravezza, M. (2017). Patterns of hydroclimatic change in the Rocky
1573 Mountains and surrounding regions since the last glacial maximum. *Quaternary*
1574 *Science Reviews*, 173, 58–77. <https://doi.org/10.1016/j.quascirev.2017.08.012>
- 1575 Singer, M. B., Asfaw, D. T., Rosolem, R., Cuthbert, M. O., Miralles, D. G., MacLeod, D., et
1576 al. (2021). Hourly potential evapotranspiration at 0.1° resolution for the global land
1577 surface from 1981-present. *Scientific Data*, 8(1), 224. [https://doi.org/10.1038/s41597-](https://doi.org/10.1038/s41597-021-01003-9)
1578 [021-01003-9](https://doi.org/10.1038/s41597-021-01003-9)
- 1579 Stansell, N. D., Klein, E. S., Finkenbinder, M. S., Fortney, C. S., Dodd, J. P., Terasmaa, J., &
1580 Nelson, D. B. (2017). A stable isotope record of Holocene precipitation dynamics in
1581 the Baltic region from Lake Nuudsaku, Estonia. *Quaternary Science Reviews*, 175,
1582 73–84. <https://doi.org/10.1016/j.quascirev.2017.09.013>
- 1583 Swinzow, G. K. (1962). Investigation of Shear Zones in the Ice Sheet Margin, Thule Area,
1584 Greenland. *Journal of Glaciology*, 4(32), 215–229.
1585 <https://doi.org/10.3189/S0022143000027416>
- 1586 Takahashi, M. (2019). Greenland’s Quest for Autonomy and the Political Dynamics
1587 Surrounding the Thule Air Base. In M. Takahashi (Ed.), *Influence of Sub-State Actors*
1588 *on National Security: Using Military Bases to Forge Autonomy* (pp. 25–49).
1589 https://doi.org/10.1007/978-3-030-01677-7_3
- 1590 Tedesco, M., & Fettweis, X. (2020). Unprecedented atmospheric conditions (1948–2019)
1591 drive the 2019 exceptional melting season over the Greenland ice sheet. *The*
1592 *Cryosphere*, 14(4), 1209–1223. <https://doi.org/10.5194/tc-14-1209-2020>
- 1593 Thomas, E. K., Hollister, K. V., Cluett, A. A., & Corcoran, M. C. (2020). Reconstructing
1594 Arctic precipitation seasonality using aquatic leaf wax $\delta^2\text{H}$ in lakes with contrasting
1595 residence times. *Paleoceanography and Paleoclimatology*, 35(7), e2020PA003886.
1596 <https://doi.org/10.1029/2020PA003886>
- 1597 USAF. (2019). THU weather observations, Thule Air Base, Greenland. 821 SPTS/OSW,
1598 USAF.
- 1599 Van Hardenbroek, M., Chakraborty, A., Davies, K. L., Harding, P., Heiri, O., Henderson, A.
1600 C. G., et al. (2018). The stable isotope composition of organic and inorganic fossils in

- 1601 lake sediment records: Current understanding, challenges, and future directions.
1602 *Quaternary Science Reviews*, 196, 154–176.
1603 <https://doi.org/10.1016/j.quascirev.2018.08.003>
- 1604 Verbruggen, F., Heiri, O., Reichert, G. J., Blaga, C., & Lotter, A. F. (2011). Stable oxygen
1605 isotopes in chironomid and cladoceran remains as indicators for lake-water $\delta^{18}\text{O}$.
1606 *Limnology and Oceanography*, 56(6), 2071–2079.
1607 <https://doi.org/10.4319/lo.2011.56.6.2071>
- 1608 Vonk, J. E., Tank, S. E., Bowden, W. B., Laurion, I., Vincent, W. F., Alekseychik, P., et al.
1609 (2015). Reviews and syntheses: Effects of permafrost thaw on Arctic aquatic
1610 ecosystems. *Biogeosciences*, 12(23), 7129–7167. [https://doi.org/10.5194/bg-12-7129-](https://doi.org/10.5194/bg-12-7129-2015)
1611 2015
- 1612 Weiss, E. D. (2001). Cold War under the ice. *Journal of Cold War Studies*, 3(3), 31–58.
- 1613 Welhan, J. A., & Fritz, P. (1977). Evaporation pan isotopic behavior as an index of isotopic
1614 evaporation conditions. *Geochimica et Cosmochimica Acta*, 41(5), 682–686.
1615 [https://doi.org/10.1016/0016-7037\(77\)90306-4](https://doi.org/10.1016/0016-7037(77)90306-4)
- 1616 Wesche, S. D., & Chan, H. M. (2010). Adapting to the impacts of climate change on food
1617 security among Inuit in the western Canadian Arctic. *EcoHealth*, 7(3), 361–373.
1618 <https://doi.org/10.1007/s10393-010-0344-8>
- 1619 Wilcox, E. J., Wolfe, B. B., & Marsh, P. (2022). Assessing the influence of lake and
1620 watershed attributes on snowmelt bypass at thermokarst lakes. *Hydrology and Earth*
1621 *System Sciences*, 26(23), 6185–6205. <https://doi.org/10.5194/hess-26-6185-2022>
- 1622 Wilcox, E. J., Wolfe, B. B., & Marsh, P. (2023). Hydrological, meteorological, and watershed
1623 controls on the water balance of thermokarst lakes between Inuvik and Tuktoyaktuk,
1624 Northwest Territories, Canada. *Hydrology and Earth System Sciences*, 27(11), 2173–
1625 2188. <https://doi.org/10.5194/hess-27-2173-2023>
- 1626